INFORMATION TO USERS

This manuscript has been reproduced from the microfilm master. UMI films the text directly from the original or copy submitted. Thus, some thesis and dissertation copies are in typewriter face, while others may be from any type of computer printer.

The quality of this reproduction is dependent upon the quality of the copy submitted. Broken or indistinct print, colored or poor quality illustrations and photographs, print bleedthrough, substandard margins, and improper alignment can adversely affect reproduction.

In the unlikely event that the author did not send UMI a complete manuscript and there are missing pages, these will be noted. Also, if unauthorized copyright material had to be removed, a note will indicate the deletion.

Oversize materials (e.g., maps, drawings, charts) are reproduced by sectioning the original, beginning at the upper left-hand corner and continuing from left to right in equal sections with small overlaps.

Photographs included in the original manuscript have been reproduced xerographically in this copy. Higher quality 6" x 9" black and white photographic prints are available for any photographs or illustrations appearing in this copy for an additional charge. Contact UMI directly to order.

ProQuest Information and Learning
300 North Zeeb Road, Ann Arbor, MI 48106-1346 USA
800-521-0600

Université d'Ottawa · University of Ottawa

NOVEL INORGANIC MEMBRANES

by

Daniel L. Brinza

A thesis submitted to the Faculty of Graduate and PostDoctoral Studies in partial fulfillment of the requirements for the degree of

Master of Applied Science in Engineering

Department of Chemical Engineering

University of Ottawa

2000

ABSTRACT

Membrane forming properties of two natural, microporous clay minerals, montmorillonite and sepiolite, were investigated. The research presented in this work was exploratory in nature and had two distinct parts: montmorillonite as a gas separation membrane material and sepiolite as an ultrafiltration membrane material. The pore size of montmorillonite was modified by pillaring with an aluminum hydroxy cation; sepiolite was only purified from its natural state. By employing the sol-gel method, with various amounts of the inorganic polymer boehmite as a binder, unsupported membranes were cast, calcined and tested under different configurations and permeating species. The membranes made of 60% pillared montmorillonite and 40% boehmite showed permeability ratios higher than 200 between gases with small molecular size (helium, hydrogen) and gases with bulkier molecules (propane, nitrogen). Preparation of composite membranes consisting of a thin layer of pillared clay/boehmite mixture on inorganic supports with different pore sizes was also attempted. The sepiolite membranes displayed a sharp pore size distribution centered around 9.3 nm radius and good results in ultrafiltration experiments using dilute aqueous solutions of macromolecules of various molecular weights. A mathematical model was attempted for the sepiolite membrane, linking pore size distribution with the experimental permeation data.

RÉSUMÉ

Les propriétés de deux argiles minéraux naturelles et microporeuses, montmorillonite et sepiolite, ont été examiné. La recherche présentée dans ce travail était exploratoire en genre et a eu deux parties distinctes: montmorillonite comme un matériel de membrane de séparation de gaz et sepiolite comme un matériel de membrane d' ultrafiltration. La taille de pore de montmorillonite a été modifiée par "pillaring" avec un aluminium hydroxy cation; sepiolite a été seulement purifié de son état naturel. En employant la méthode de sol-gel, avec des quantités diverses du polymer inorganique boehmite comme un liant, les membranes non soutenues ont été moulées, calcinées et testées sous les configurations et l'espèces de permeation différente. Les membranes fait de 60% pillared montmorillonite et 40% boehmite ont montrées les proportions de permeabilité plus hautes que 200 entre les gaz avec la petite taille moléculaire (l'hélium, l'hydrogène) et les gaz avec les molécules plus volumineuses (le propane, l'azote). La préparation de membranes composées consistant en une couche mince de mélange d'argile/boehmite de pillared sur les soutiens inorganiques avec les tailles de pore différentes a été aussi tentée. Les membranes de sepiolite ont montré une distribution de taille de pore aiguë, concentré environ 9.3 nm (rayon) et des bons résultats dans les expériences de ultrafiltration en utilisant des solutions aqueuses diluées de macromolecules de poids moléculaires diverses. Un modèle mathématique a été tenté pour la membrane de sepiolite, qui relie la distribution de taille de pore avec les données de permeation expérimentales.

ACKNOWLEDGMENTS

I would like to express my sincere gratitude to Professor Takeshi Matsuura for giving me the chance to join his group. I enjoyed working under his supervision. I thank him for his understanding, patience and constant guidance and encouragement.

I would also like to thank the members of the Industrial Membrane Research Institute at the University of Ottawa, in particular Dr. Geeta Chowdhury, for their help, friendship and insightful discussions over the course of my studies. I feel very fortunate to have had the chance to meet and work with so many talented people.

I enjoyed working on a joint project with Professor's Christian Detellier group from the Department of Chemistry, University of Ottawa and thank him and all those involved for their help.

I would also like to thank the faculty members and the staff of the Department of Chemical Engineering, University of Ottawa.

Finally, the financial support of NSERC, Government of Ontario (Ministry of Training, Colleges and Universities), University of Ottawa and Department of Chemical Engineering is gratefully acknowledged.

NOMENCLATURE

c - solute concentration in the feed (ppm)

c_p -solute concentration in the permeate (ppm)

f(r) - distribution function for the pore radius.

j(r) - volumetric flux through a single pore (m^3/s)

D – Diffusivity (m^2/s)

J - total membrane flux (m^3/s)

L - membrane thickness (m)

M, M_w - molecular weight of a polymer (kg/kmol, a.k.a. Dalton)

ΔP - transmembrane pressure (Pa)

T - temperature (K)

r - pore radius (m)

$\bar{r}$ - average pore radius (m)

a_i - Einstein-Stokes radius of i^{th} solute molecule (m)

r_i - radius of the largest pore blocked by the i^{th} solute molecules (m).

Greek Letters

η - viscosity (Pa s)

$[\eta]$ - intrinsic viscosity of a solute (m^3/kg)

σ - geometric standard deviation of the log-normal distribution (dimensionless)

Abbreviations

PEG - poly (ethylene glycol)

PEO - poly (ethylene oxide)

PR_i - permeation flux corresponding to i^{th} solute (l/m^2 h)

PWP - pure water permeation flux (l/m^2 h)

$(Sep)_i$ - separation for a solute "*i*" (dimensionless)

TABLE OF CONTENTS

LIST OF TABLES

Number *Page*

LIST OF FIGURES

Number *Page*

CHAPTER 1. INTRODUCTION

1.1 Scope of research

Inorganic membranes are a relatively new addition to the mainstream of membrane research, despite the evidence that shows some studies on inorganic membranes such as platinum and porous glass as early as 19th century. Recent years have seen a tremendous growth in research and development efforts in this field and even the introduction of many commercial ceramic membranes to a market dominated, almost exclusively, by organic polymeric membranes. Their higher thermal and chemical stability are the two most important areas in which inorganic membranes compare very favourably with their organic counterparts.

The operable temperature limits of inorganic membranes are obviously much higher than those of organic polymeric membranes. Most organic membranes begin to deteriorate structurally above 100 °C, which is rarely the case with inorganic membranes. Thermal stability of membranes is not only a technical problem but also an economic issue. For example, when membrane separation is to be applied to a hot process stream, the need to ramp down the temperature (to maintain the physical integrity of an organic membrane) and to ramp up the temperature again after separation can be eliminated with the use of a temperature resistant inorganic membrane.

Inorganic membranes can (with few exceptions) withstand organic solvents, chlorine and other chemicals better than organic membranes. This makes them a preferred choice for processing non-aqueous solvent streams and it also permits the use of more effective and yet corrosive cleaning procedures and chemicals.

Many organic membranes are susceptible to microbial attack during applications. This is not the case with inorganic types, particularly ceramic membranes. In addition, inorganic membranes in general do not suffer from the mechanical instability of many organic membranes where the porous support structure can undergo compaction under high pressures and cause decrease in permeability. It is obvious that in a high temperature or oxydizing environment, inorganic membranes could become the only acceptable solution to many challenging separation applications.

Their higher thermal and chemical stability not only make inorganic membranes very suitable for separation applications, but also for reaction enhancement. A membrane can act as an active participant in a chemical transformation if placed in such a configuration that the membrane not only plays the role of a separator but also of a part of the reactor's wall. This dual use of an inorganic membrane as a separator and as a reactor wall offers great promises for conversion enhancement of equilibrium reactions. With their better thermal stability than organic membranes, inorganic membranes are attractive candidates for many industrially important chemical reactions that are frequently operated at high temperatures and, in some cases, under harsh chemical environments.

Despite all the recent inroads into the mainstream commercial market, inorganic membranes, especially gas separation membranes, are still at an early stage of development and far from reaching the degree of maturity required to become widely accepted. The

choices offered with regards to membrane material, pore size distribution, element shape, end seal material, design and module configuration are still limited today. As more research and development efforts are directed to these areas of limitations - as witnessed worldwide today - inorganic membranes are expected to become more technically feasible and economically viable in an increasing number of applications.

This thesis is a part of the ongoing search for new inorganic membranes and membrane materials of practical significance. Its first and foremost goals were of an exploratory nature, towards the discovery of new membrane materials based on microporous clay minerals. Should a good membrane forming material be found, a primary goal was to prepare robust membranes, then summarily characterize and test them for gas and liquid separation. Should a good gas separation membrane be found, an optional goal was to investigate the possibility of using it in a membrane reactor configuration of some kind, preferably a catalytic membrane reactor.

1.2 Background Information

The following two natural clay minerals were of particular interest to us: montmorillonite (layered clay from the smectite family) and sepiolite (fibrous clay).

1.2.1 Montmorillonite and the smectites.

Smectites are a part of the larger family of 2:1 type clay minerals. The 2:1 clay minerals are all comprised of an octahedral metal (usually Al or Mg) oxide sheet sandwiched between two tetrahedral silicate sheets (Figure 1.1). Isomorphic substitution of one metal for another lower valent metal in either the tetrahedral sheets or the octahedral sheet may impart a net negative charge to the 2:1 layers. In smectites, this negative layer charge is counterbalanced by exchangeable interlayer hydrated cations such as Na^{+}.

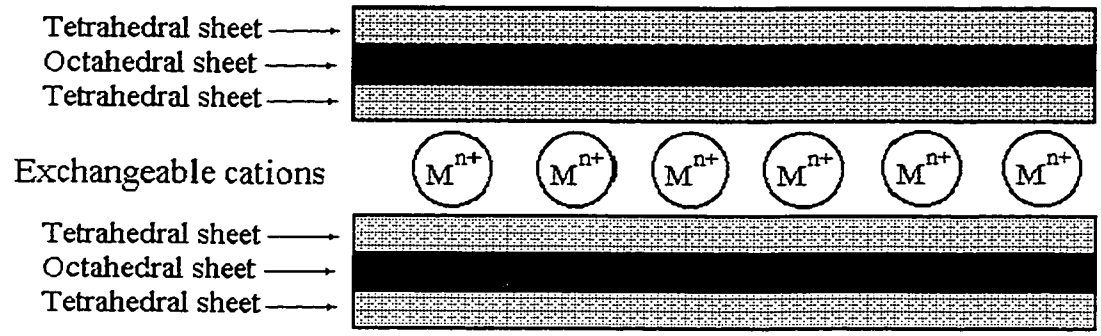

Figure 1.1. Smectite Structure of Montmorillonite

There are two main subgroups within the smectite group: the dioctahedral smectites of which montmorillonite is a member, and the trioctahedral smectites. In dioctahedral smectites, only 2/3 of the octahedral sites are occupied, usually by Al^{3+} cations, leaving every third octahedral site vacant. For trioctahedral smectites, all of the octahedral sites are occupied, usually by Mg^{2+} cations. The clay mineral used in this project, montmorillonite, is comprised principally of Al^{3+} in the octahedral sheet with some isomorphic substitution by Mg^{2+}.

One of the most striking features of smectite clays is the ability of these clays' layers to swell, and for the interlayer hydrated cations to be exchanged with a wide assortment of cations. These cations may be other hydrated metal cations (Li^+, K^+, Cu^{2+}, Fe^{3+} etc.), organic cations (such as alkyl ammonium), or various complex inorganic hydroxy cations.

Figure 1.2 shows the exchange of interlayer Na^+ cations with the large $[Al_{13}O_4(OH)_{24}(H_2O)_{12}]^{7+}$ cluster-ion (which, because of its long formula, is usually abbreviated as $[Al_{13}]^{7+}$ or referred to as Keggin Ion) to give an $[Al_{13}]^{7+}$ exchanged smectite. By calcination, these interlayer clusters become rigid, stable aluminum oxide pillars that hold the layers apart at subnanometer distance, thus creating galleries of molecular size. Calcination involves prolonged thermal treatment at temperatures above 500 °C with the purpose of turning all inorganic chemical species into stable, insoluble metal oxides.

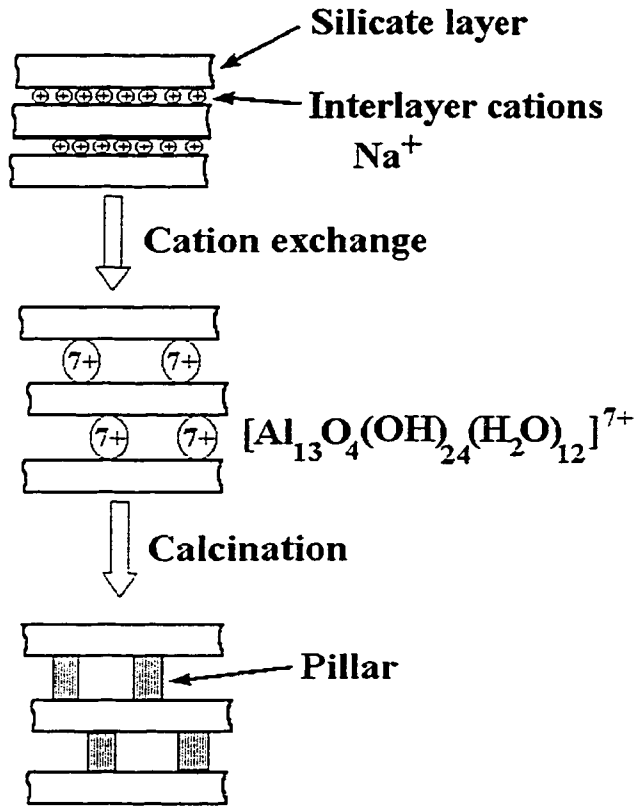

Figure 1.2. Pillaring of a Smectite Clay with the Keggin Ion.

1.2.2 Sepiolite

Sepiolite is a natural hydrated magnesium silicate mineral, which consists of fibrous talc-like layers stacked in long ribbons, with micro-channels and grooves parallel to the fibre axis. Channel dimensions are 3.7Å x 10.6Å (as shown in Figure 1.3). An ideal elemental formula for sepiolite can be given as: $Mg_8Si_{12}O_{32} \cdot n(H_2O)$. Its schematic structure is shown in Figure 1.3. The presence of micropores and channels in this mineral, together with the fine particle size and fibrous habit, accounts for its high surface area.

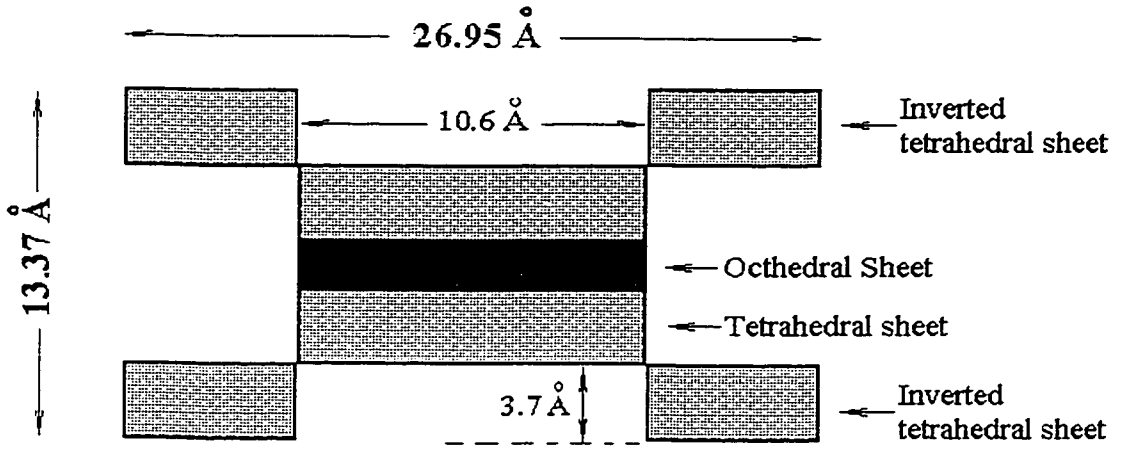

Figure 1.3. Schematic Structure of Sepiolite Elementary Unit

Theoretically, by repeating itself towards the three dimensions, the elementary unit shown in Figure 1.3 above creates a crystal containing molecular size pores, as shown in Figure 1.4 below:

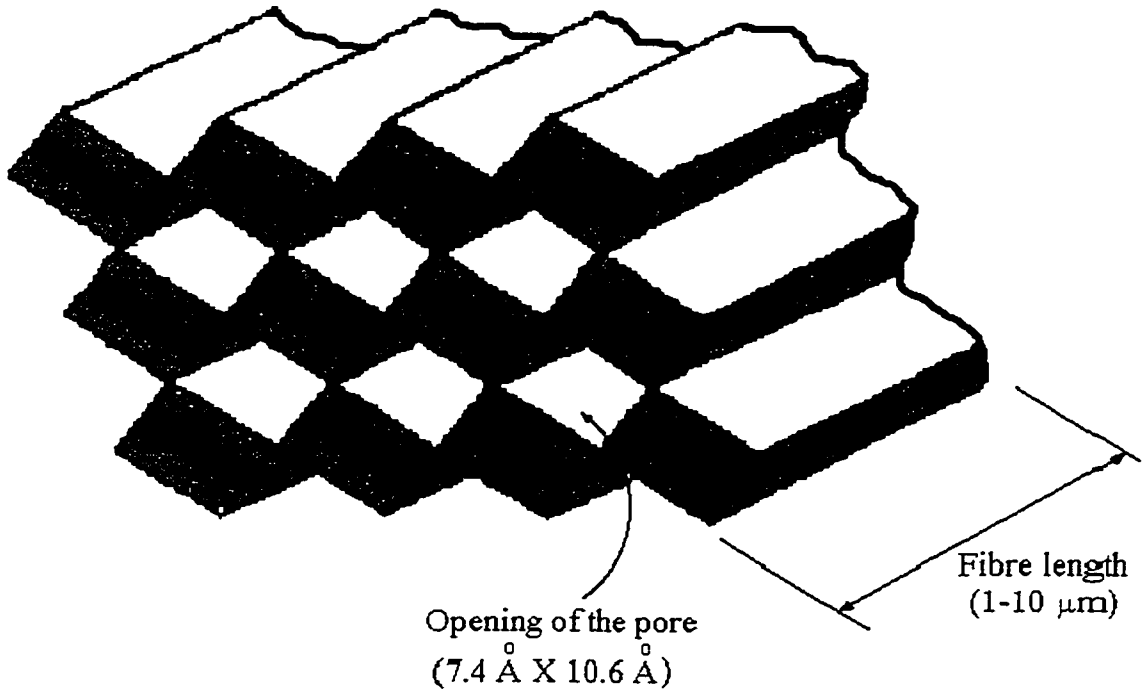

Figure 1.4. Theoretical Structure of a Sepiolite Crystal

In natural sepiolite, the structure shown in Figure 1.3 does not repeat itself equally towards all three dimensions. One direction (perpendicular to the page) is more favored, so that the final macroscopic crystals are actually fiber-shaped, 1-10 μm in length and 5-50 nm in diameter. Figure 1.4 also shows clearly the existence of well-defined, regular micropores running parallel to the fiber's axis. It was these pores that qualified sepiolite as a potential candidate for a good gas separation membrane and as an object of this research project.

1.3 Survey of the recent literature

1.3.1. Pillared Clays

The literature concerning the use of pillared clays in inorganic membranes is very sparse. An exhaustive literature search resulted in only three journal articles pertaining to this subject.

In the first paper (Lao et al.. 1994). a microporous unsupported inorganic $[Al_{13}]^{7+}$ pillared clay membrane was prepared by an alumina sol-gel process. It was shown that the microporosity of the pillared clay material (pore size was 8-9 Å in diameter) could be retained in the sol-gel composite membrane. Significantly, as the loading of the $[Al_{13}]^{7+}$ pillared montmorillonite increased in the membrane. the ratio of micropore volume to mesopore volume increased.

In the second example (Hu et al., 1994), an Al_{13} pillared clay-composite membrane was prepared by multi-depositing alumina pillared clay and carbon on a macroporous glass support. The calcination of the Al_{13} pillared clay was done at 500 °C and at least five deposition/calcination cycles were required until the interparticle pore size were acceptable and cracks were eliminated. In order to block the large interparticle pores still present, carbon was deposited in a final step through the carbonization of polyvinyl alcohol (PVA) at 450°C under vacuum.

The prepared membrane was then tested for its separation of nitrogen/organic vapour mixtures, under both static and dynamic conditions. The separation process proved most effective for the static separation, where samples containing a gas mixture were

simply allowed to permeate through the membrane into a previously evacuated flask. For both separation processes, it was found that the efficiency of the separation was: benzene > toluene > o-xylene > 1,2-dichlorobenzene. This result suggests that the larger the permeating molecule is, the stronger the interaction between the composite membrane and that molecule is, resulting in a reduced ability of that molecule to diffuse through the membrane. The authors explained the separation mechanism based on Knudsen diffusion and not on molecular sieving effects.

In the third example (Vercauteren et al., 1996; Vercauteren et al., 1998) an Al_{13} pillared clay-composite membrane was prepared by first dip-casting an ultrathin layer of clay on a home-made γ-alumina support, followed by the pillaring reaction, washing, drying and calcination. The thickness of the clay layer was easily controlled by varying the dipping time of the γ-alumina supports into the clay suspension.

Crack free and pinhole free composite membranes were thus obtained, exhibiting very low permeation rates compared to the initial γ-alumina supports. Unfortunately, their H_2/N_2 permselectivity was the same as for the γ-alumina supports, regardless of the pillared clay layer thickness, result that was attributed by the authors to an incomplete pillaring of the top clay layer.

1.3.2. Sepiolite

Although there has been a considerable number of studies on sepiolite devoted to structural analysis (Caillere et al., 1961; Ahlrichs et al., 1975; Grillet et al., 1988), surface and adsorption characteristics (Fernandes-Hernandes et al., 1979; Rubica, 1985), dehydration behaviour (Nagata et al., 1974; Rautureau and Tchoubar, 1976; Fernandes-Alvares, 1978), rheological and catalytic properties (Corma et al., 1984; Santaren, 1993; Simonton et al., 1998), sintering and hydrothermal sintering (Fukushima et al., 1993; Goktas et al., 1997; Baykara et al., 1997), to the best of our knowledge, no research on sepiolite as a membrane material has ever been published.

Chapter 2. THEORETICAL ASPECTS

2.1 Permeability and Selectivity Equation for Gas Separation

The permeability (P) of a membrane with respect to a given permeating species is given by Equation 2.1 below:

$$P = \frac{Q \cdot d}{A \cdot \Delta p} \qquad 2.1$$

where

Q is the molar permeation rate (mol/s)

d is the membrane thickness (m)

A is the membrane surface area (m^2)

Δp is the pressure difference across the membrane (Pa)

The unit of permeability P is thus (mol/s·m·Pa).

Very often for gases and vapours, permeability (P) is also expressed in terms of a unit known as the "Barrer", using the following equation:

$$P = \frac{V \cdot d}{A \cdot \Delta p} \qquad 2.2$$

Where

V is the volumetric permeation rate (cm^3(STP)/s)

d is the membrane thickness (cm)

A is the membrane surface area (cm^2)

Δp is again the pressure difference across the membrane (cm Hg)

The unit "Barrer" is 10^{-10} cm^3(STP)·cm/cm^2·s·(cm Hg) which can be simplified to 10^{-10} cm^2/s·(cmHg).

The permeance of a membrane is related to its permeability P by Equation 2.3:

$$Permeance = \frac{Permeability}{Membrane\ Thickness} = \frac{P}{d} \qquad 2.3$$

Permeance is similar to permeability, except that the membrane thickness is not factored in. Permeance may be expressed in units of (mol/s·m^2·Pa) or (Barrer/cm).

The dimensionless ratio α between the permeabilities measured for two gases in similar conditions but in two separate single permeation experiments is sometimes referred to as an "ideal separation factor" and may or may not reflect accurately the behaviour of the membrane under mixed feed conditions. The ideal separation factor α is calculated from Equation 2.4:

$$\alpha = \frac{P_A}{P_B} \qquad 2.4$$

where P_A and P_B are the permeabilities of gases A or B measured in identical conditions but in two separate single permeation experiments. For a new membrane material, a high value for the ideal separation factor would be a very good preliminary result and it would warrant further experiments under mixed feed conditions.

2.2 Modelling of Sepiolite Membrane Pore Size Distribution Based on Ultrafiltration Results

The first important assumption of the model is that membrane pore size follows a log-normal distribution characterised by the distribution function f(r) shown below:

$$f(r) = \frac{1}{r\sqrt{2\pi}\ln(\sigma)} \exp\left\{ - \frac{\left[\ln(r) - \ln(\bar{r})\right]^2}{\left[\ln(\sigma)\right]^2} \right\} \qquad 2.5$$

where: f(r) is the distribution function for the pore radius.

r is the pore radius (nm)

$\bar{r}$ is the average pore radius (nm)

σ is the geometric standard deviation of the log-normal distribution.

The second important assumption of this model is partial pore blocking by the solute. Solute molecules are assumed to be rigid spheres with a radius equal to Stokes radius a_i. Depending on the membrane pore radii, the following three situations are presumed possible:

1. Pores having radii smaller than a_i cannot be entered by the solute molecules but remain fully open for solvent (water) passage.
2. Pores having radii equal or larger than a_i, up to a size r_i, are completely plugged by the solute molecules that enter them. No mass transport takes place through these pores.

3. Very large pores, i.e. pores with radii larger than r_i, are fully open for unhindered solute and solvent transport.

Blocked pores are represented by the grey area in the Figure 2.1 below.

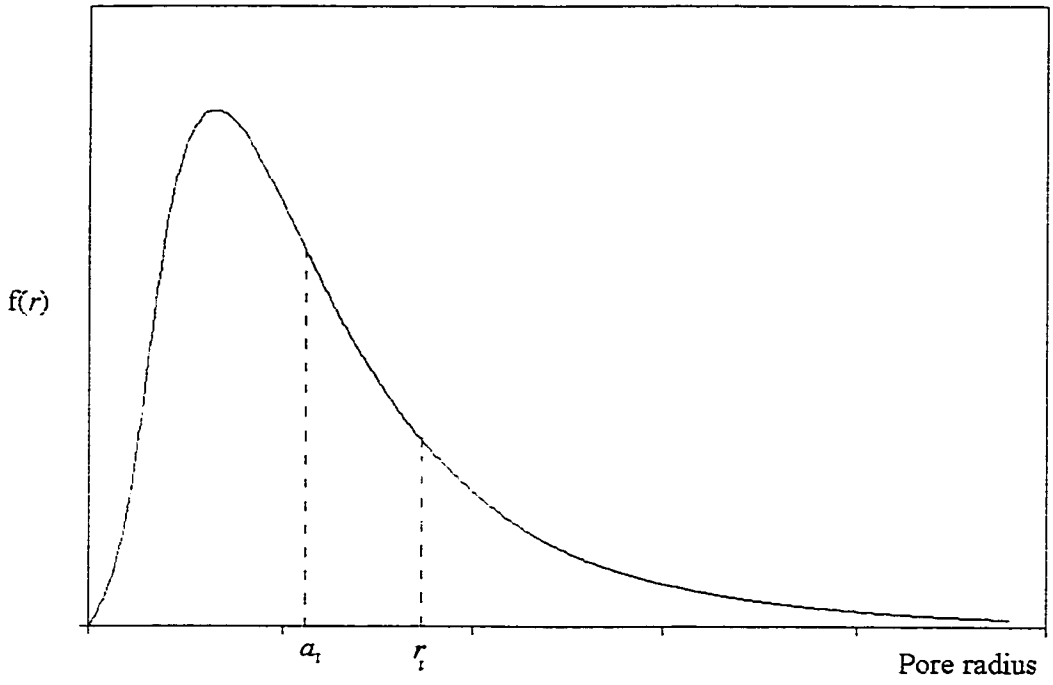

Figure 2.1. Log-Normal Distribution of Sepiolite Membrane Pore Size in Relation with Solute Molecule Size:

a_i is the Stokes radius of i^{th} solute.

r_i is the maximum size of a pore blocked by i^{th} solute.

The following assumptions are made:

-membrane pores are cylindrical;

-membrane thickness is uniform;

-solution is dilute enough that its viscosity can be considered approximately equal to the pure solvent's viscosity

-laminar flow through the pores (Re < 2000);

-no interaction between solute and membrane surface;

-no concentration polarisation takes place;

-no solvent drag effects on solute;

-no resistance due to the sharp edge of the pore entrance;

-pure sieving mechanism for separation;

Under these conditions, the Poiseuille flow model correlates the volumetric flow rate through a pore and the pore radius by Equation 2.6:

$$j(r) = (\pi \Delta P / 8 \eta L)\, r^4 \qquad 2.6$$

where: j(r) is the volumetric flux through a pore (m^3/s)

r is the pore radius (m)

ΔP is the transmembrane pressure (Pa)

η is the solution viscosity (Pa s)

L is the membrane thickness (m)

In the case of pure water permeation, all pores are available for transport, thus the total flux through all pores J, can be written as:

$$J = \int_0^{\infty} j(r)\, f(r)\, dr \qquad 2.7$$

where: $f(r)$ is the distribution function for the pore radius.

In the case of permeation of a solute "*i*" having molecules of radii a_i, some pores (i.e. pores with radii between a_i and r_i) are assumed blocked; thus the total flux through all pores Jp_i can be written as:

$$J_{p_i} = \int_0^{a_i} j(r)\, f(r)\, dr + \int_{r_i}^{\infty} j(r)\, f(r)\, dr \qquad 2.8$$

where: a_i is the Stokes radius of i^{th} solute (m)

r_i is the maximum size of pores blocked by i^{th} solute (m).

i=1, 2, ...n *i=1* refers to the first solute used.

i=2 refers to the second solute used.

i=n refers to the n^{th} solute used.

For experiments performed under identical conditions, the ratio of permeation rate corresponding to i[th] solute PR_i to pure water permeation rate PWP can be therefore written as:

$$\frac{\int_0^{a_i} j(r)\, f(r)\, dr + \int_{r_i}^{\infty} j(r)\, f(r)\, dr}{\int_0^{\infty} j(r)\, f(r)\, dr} = \left(\frac{PR}{PWP}\right)_i \qquad 2.9$$

$i=1, 2, \ldots n$

After simplification, the following final equation is obtained:

$$\frac{\int_0^{a_i} f(r)\, r^4\, dr + \int_{r_i}^{\infty} f(r)\, r^4\, dr}{\int_0^{\infty} f(r)\, r^4\, dr} = \left(\frac{PR}{PWP}\right)_i \qquad 2.10$$

$i=1, 2, \ldots n$

For a solute "i" separation $(Sep)_i$ can be defined as follows:

$$(Sep)_i = \frac{c - c_p}{c} \qquad 2.11$$

where: c is solute concentration in the feed (ppm)

c_p is solute concentration in the permeate (ppm)

$i=1, 2, \ldots n$

The average concentration c_p of a solute in the permeate stream can be expressed as in Eq. 2.12 below:

$$c_p = \frac{solute\ flux}{solvent\ flux} = \frac{\int_{r_i}^{\infty} c\, f(r)\, r^4 dr}{\int_0^{a_1} f(r)\, r^4 dr + \int_{r_i}^{\infty} f(r)\, r^4 dr} \qquad 2.12$$

$i=1, 2, \ldots n$

Thus the expression for separation becomes:

$$1 - \frac{\int_{r_i}^{\infty} f(r)\, r^4\, dr}{\int_{0}^{a_i} f(r)\, r^4\, dr + \int_{r_i}^{\infty} f(r)\, r^4\, dr} = (Sep)_i \qquad 2.13$$

$i=1, 2, \ldots n$

Eq. 2.10 and Eq. 2.13 together form a set of (2n) equations with (n+2) unknowns. The unknowns are:

r_i the maximum size of a pore blocked by i^{th} solute (n unknowns, $i=1,2\ldots n$)

$\bar{r}$ the average pore radius

σ the geometric standard deviation of the log-normal distribution.

Chapter 3. METHODOLOGY

There are so many techniques employed in the preparation of inorganic membranes that even a brief description of each of them would make enough material for a book. For the purpose of this project, a starting point was the general observation that many available inorganic materials, such as pillared smectites and zeolites, have interesting microporous structures (pore diameters less than 20 Å) but they exist as powders in the bulk macroscopic state. In order to take advantage of the porous structure of these materials for use in membranes, one must find a way to prepare these materials as robust films.

This may be accomplished by two approaches:

a) an *in situ* approach that aims at crystallizing these materials directly in the form of either a supported or an unsupported membrane. Membranes prepared by this approach would, ideally, have the whole permselective layer actually made up of a single megacrystal that extends greatly on two dimensions and minimally on the third dimension (ultrathin crystalline sheet). While this defect-free monocrystal coverage has not yet been achieved on a large scale, continuously crystalline coatings resulting from the intergrowth of many smaller crystallites are now commercially available on a variety of porous supports. Ongoing research in this direction (Vroon et al., 1996; Kusakabe et al., 1996; , Liu et al., 1997; Yan et al., 1997; Kondo et al., 1997; Boom et al., 1998; Vroon et al., 1998; Kusakabe et al., 1998; Piera et al., 1998; Chau et al., 2000) focuses on reducing the thickness of these crystalline layers (to maximize

permeation rates) and on minimizing the occurrence of defects (to maximize selectivity).

b) a preassembled approach that consists in preparing first the porous material as a fine uniform powder and then either crosslinking the individual particles or incorporating the material in a suitable, film-forming matrix.

For the purpose of this thesis, the second approach (preassembled) was considered more suitable, especially since the materials of interest for the present project were clays readily found in the nature as powders or loose agglomerates. Moreover, while artificial crystallisation of these two particular materials is reported in the literature, the extreme complexity and low yields reported make the *in situ* approach inapplicable to montmorillonite and sepiolite.

The general methodology used throughout this thesis can be summarised as follows:

1. Select and purify clay materials with well-defined natural or induced microporosity.
2. Fractionate and retain the finer fraction (particle size smaller than 0.2μm).
3. Intimately mix the appropriate clay suspension with the binder (boehmite sol) in various ratios (from 0% to 100% clay).
4. Cast the suspension on a flat surface following a "classic" sol-gel procedure.
5. Air dry followed by calcination and testing.

3.1 Sol-gel Method for Preparing Inorganic Membranes

In recent years, the sol-gel method has been extensively developed for the preparation of micro- and mesoporous inorganic membranes. Alumina, silica, zirconia, titania and mixed oxide systems have all been explored as appropriate membrane systems and intensive research on these systems continues (Vacassy et al., 1998; Seshadri et al., 1998; Bjorkert et al., 1998; Schlottig et al., 1998; Pan et al., 1999; Kusakabe et al., 1998; Lee et al., 1999; Schaep et al., 1999; Cheong et al., 1999; Xia et al., 1999; Schlottig et al., 1999; Zhua et al., 1999; Kusakabe et al., 1999; Honma et al., 1999; Schiza et al., 1999; Seshadri et al., 1999; Shi et al., 1999; Bjorkert et al., 1999). The sol-gel technique involves the use of a metal alkoxide precursor, which is hydrolyzed in a controlled manner, yielding water-soluble mono- and polyhydroxylated inorganic species. Upon aging and heating, polycondensation reactions take place between these species, resulting in densely branched inorganic macromolecules. These macromolecules are not soluble in water but individually they structure themselves as tightly packed coils to form a stable, viscous colloidal sol in which water is the dispersion medium. A sol is still a liquid and it can be cast or made to take the shape of any vessel or mold. Further drying causes the condensation reactions to proceed three-dimensionally and individual colloidal particles assemble together in highly crosslinked chains. At this point the system becomes a gel; the crosslinked inorganic polymer is the dispersion medium while water is just being held in the interstitial space. A gel is a semi-solid system that holds its shape and has a structure with a certain degree of rigidity. Upon complete drying and/or calcination, this gel turns into a solid metal oxide matrix (Figure 3.1).

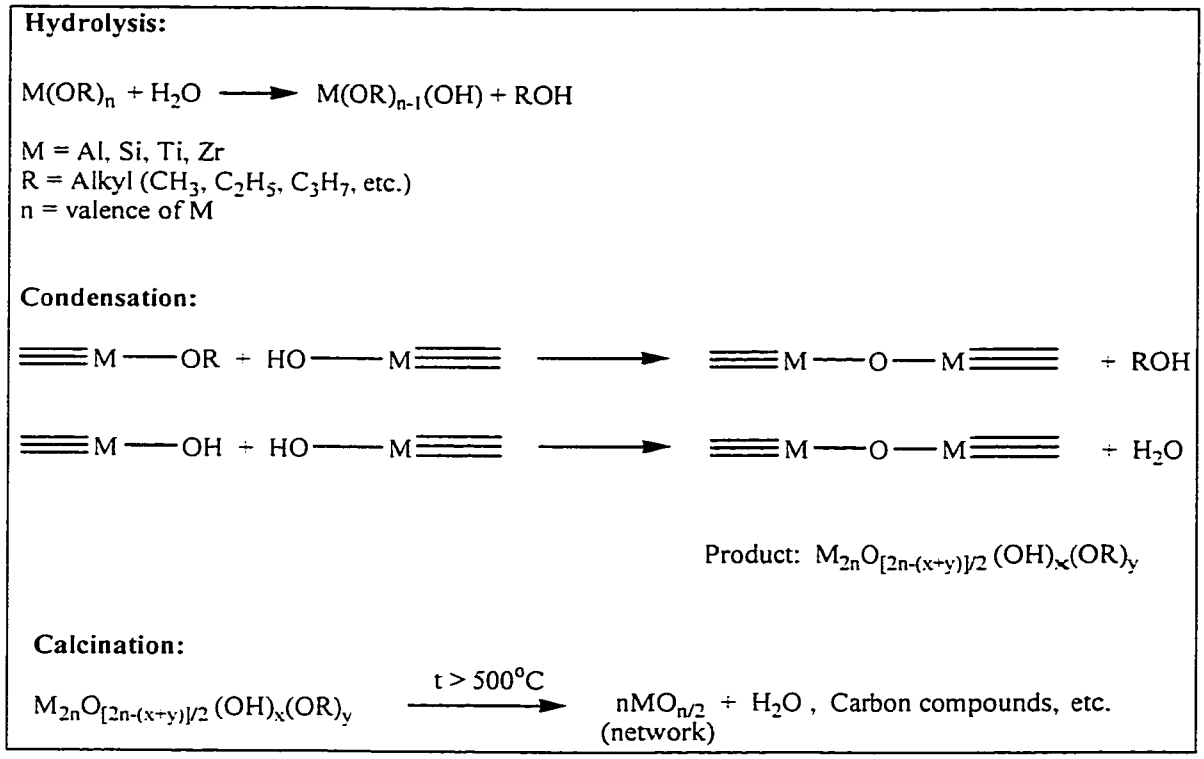

Figure 3.1. Sol-Gel Process Starting from a Metal Alkoxide $M(OR)_n$

(adapted from Lao, 1994)

By manipulating several parameters in the synthesis described above, the final macroscopic texture of this rigid three-dimensional metal oxide mass can be adjusted to be as porous as a sponge, or as dense as a solid slab of glass (monolith), or almost everything between these two extremes. The sol-gel method offers considerable flexibility in the preparation of inorganic membranes, since structural control can be imparted to the final

membrane material by varying parameters like metal alkoxide precursor or the conditions of hydrolysis and drying.

The alkoxide precursor can be varied by either changing the metal or the ligands on the metal. Varying the stoichiometry of the amount of water added during hydrolysis affects the degree of cross-linking. Some additives, such as inorganic acids and bases, may catalyze the sol-gel process whereas others, such as carboxylic acids (acetic acid and propionic acid), may actually inhibit hydrolysis in some sol-gel processes. Finally, the method of drying (i.e. freeze drying, supercritical drying, microwave drying etc.) and the temperature of drying have pronounced effects on the final textural properties.

Aside from being used alone to prepare metal oxide membranes, the sol-gel technique has also been used in the preparation of the inorganic matrix to support and impart mechanical stability to other microporous inorganic materials such as zeolites for use as chemical sensors. This has also recently been tried with pillared clays.

For the purpose of this thesis, aluminum tri(*sec*-butoxide) with formula $Al(OC_4H_{10})_3$ was the metal alkoxide of choice. When processed according to the sol-gel method outlined above, the hydrolysis and polycondensation product of this alkoxide is an inorganic polymer known as "boehmite" with the repeating unit of formula AlOOH. Throughout this thesis the term "boehmite sol" refers to this colloidal sol; upon drying this sol turns into a gel and upon calcination it forms the tri-dimensional aluminum oxide (Al_2O_3, alumina) network that acts as a binder for the clay particles.

Figure 3.2 shows the intended structure that the composite membranes were supposed to have after calcination: microporous clay particles embedded in an alumina

matrix that should impart structural resistance and force all permeating species to pass at least once through a microporous domain where molecular sieving would take place.

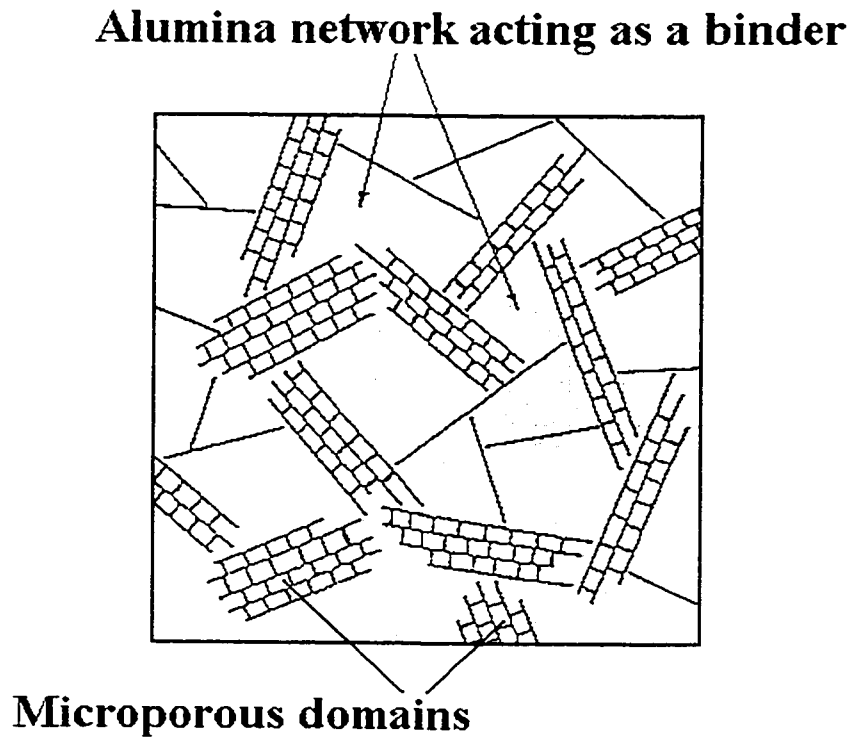

Figure 3.2. Structural Design of the Composite Membranes

Chapter 4. PROPERTIES OF MATERIALS

4.1 Materials

All chemicals (described in Chapter 5) were of reagent grade quality and were used without additional purification unless indicated. Montmorillonite (coded MWy-2) was obtained from the Source Clay Repository of the Clay Minerals Society (Department of Geology, University of Missouri, USA). MWy-2 is a Na^+ montmorillonite (Na^+-M) and is originated from Crook County, Wyoming (hence the code name: **M**ontmorillonite **Wy**oming). A more complete description of this clay is given in Chapter 5. The as received clay had to be purified in order to remove carbonates, coarse clay fractions and other impurities before proceeding with pillaring (Section 5.2).

Sepiolite (coded SNe-1) was also obtained from the Source Clay Repository of the Clay Minerals Society (Department of Geology, University of Missouri, USA). SNe-1 is originated from Nevada (hence the code name: **S**epiolite **Ne**vada).

The dialysis bags which were used to wash the clays free of soluble salts were made from natural cellulose (SpectraPor 2 Molecularporous Dialysis Membranes) and had a molecular weight cut-off (MWCO) value of 12-14,000, a flat width of 45 mm and a diameter of 29 mm. The dialysis bags could be reused many times, and when not in use, were stored in a 1% formaldehyde solution to prevent microbial decomposition, as suggested by the manufacturer.

Porous α-alumina disks and tubes were Hytrex® brand from Osmonics Inc. (Minnetonka, MN, USA). The disks had a thickness of 3.2 mm, a diameter of 3.8 cm and a pore size of 0.2 μm. The tubes had an outside diameter of 2.54 cm, wall thickness of 3.2 mm and came in the following pore sizes: 0.1 μm, 0.3 μm, 0.7 μm and 1.0 μm. The length of the tubes was 20 cm but, to facilitate the coating and testing, slices of 3 cm in length were used for each membrane, cut off from the larger tube with a hacksaw. Hytrex® tubes and disks have a homogeneous (symmetric) structure resulting from their manufacturing method (cold isostatic pressing of α-alumina particles into the desired shape followed by sintering at temperatures greater than 1200°C, when a uniform matrix of permanently bonded together particles forms).

4.2 Characterisation Techniques

4.2.1 XRD

Powder X-ray diffraction (XRD) patterns were obtained on a Philips PW 3710 diffractometer using a generator voltage of 45 kV and a generator current of 40 mA. Typically, a step size of 0.04 °2θ was used with a dwell time of 0.5 seconds per step. The sample was spun during the acquisition, and an automatic divergent slit and a 0.1 mm receiving slit were used without employing any masks. Oriented samples were prepared by dispersing a small amount of powder (20-30 mg) in approximately 1-2 mL of water followed by application and air drying on a glass XRD slide. Sonication (1-2 minutes) was

sometimes used to aid in the dispersion of the powder. The d_{001} values or the basal spacing of the clays were calculated automatically as the maximum of the smoothed peak using the Philips peaksearch software. The linewidth of the reflections was calculated as the full width at half maximum (FWHM) and is given in °2θ units.

4.2.2 Particle Size Analysis

Particle size analysis was done on a Micromeritics Sedigraph 5100. A solution of 0.05% sodium metaphosphate in water was used as both the background liquid and as dispersant liquid for the clay materials. Approximately 1.0 g of material in 40 mL of 0.05 % sodium metaphosphate solution was required to be in the optimal detection range of the machine. The densities of the materials were taken to be 2.54 g/cm^3 in accord with the reported density of clays.

4.2.3 Total Organic Carbon Analysis

A total organic carbon analyser (Shimadzu Corporation TOC-5050) was used to analyse the total carbon content in ultrafiltration samples. The analyser is capable of detecting organic carbon at concentration levels as low as 10 ppb. It is fully automatic and is capable of performing a self-calibration. A few standard PEG and PEO solutions ranging in concentration from 100 ppm to 0.1 ppm were prepared and used for calibration since results in this stated range were anticipated from the analysis.

Chapter 5. EXPERIMENTAL ASPECTS

5.1 Purification of Clays

5.1.1 Montmorillonite (MWy-2)

An amount of 30g of crude MWy-2 was stirred overnight in 500 ml of distilled water. In order to destroy any carbonates that may be present as impurities, 1 M HCl was added under vigorous stirring until a pH of 3.5 could be maintained constant after at least 15 minutes. The suspension was then centrifuged in 250 ml centrifuge bottles (20 minutes at 3000 rpm), and the clear supernatant solution was discarded. The remaining sediment was redispersed in dilute HCl (pH=3.5) and again centrifuged. Four such cycles (centrifugation - supernatant discarding - sediment redispersion) were deemed necessary for the complete removal of all soluble species resulted from the acid decomposition of the carbonates (the fifth supernatant tested negative for Ca^{2+}, Mg^{2+} and Na^{+} ions).

The entire procedure mentioned in the paragraph above was repeated with another batch of 30 g of crude MWy-2 clay. The products of both batches were combined in a large (4 litre) beaker; water was added to give a total volume of 3.6 litres, and the pH was adjusted to 8-9 by adding small amounts of a 0.1 M solution of NaOH. The suspension was vigorously stirred for 1 hour followed by sedimentation to remove the particles of less than 0.2 μm e.s.d. (equivalent spherical diameter). After 16 hours of sedimentation time all particles greater than 0.2 μm e.s.d. should have settled below 20 cm from the surface, so the top 20 cm of the supernatant (containing the finest clay fractions) was siphoned and collected. The remaining sediment was redispersed in water to the 3.6 litre mark then

sonified for 10 s and allowed to settle again for 16 hours. The sediment was discarded while the top 20 cm portion of the supernatant from this second sedimentation procedure was collected and combined with the similar fraction from the first sedimentation in a large (6 litre) Erlenmeyer flask. The pH of this suspension was adjusted to 3.5 with 1 M solution of HCl and then 250-300 g of solid NaCl was added under stirring. This caused the suspended clay particles to flocculate and settle to the bottom of the flask. Also, the large excess of NaCl in solution resulted in a complete replacement (exchange) of all other naturally present interlayer cations with Na^+ cation.

After standing overnight, the clear supernatant solution was discarded, and the flocculated sediment was collected and placed in dialysis bags. The dialysis bags were then placed in a large container of deionized water (volume = 6 litres) and the water was frequently changed over the course of 7-14 days. When the water surrounding the dialysis bags tested negative for Cl^- ions using a saturated $AgNO_3$ solution (meaning that all the excess ionic species had been completely washed away) the contents of the bags were transferred to a thick walled flask and freeze dried. After freeze drying, a fluffy, off-white, pure homoionic Na^+ montmorillonite (Na^+-M) was collected. Overall, the yield of purified clay was 20-25% starting from the crude MWy-2.

The material thus purified underwent characterization by XRD and particle size analysis. XRD analysis confirmed that the d-spacing of the purified MWy-2 was 12.5 Å, which is what one expects for a hydrated sodium montmorillonite. Comparison of the crude and purified samples showed that most of the quartz impurities had been removed through sedimentation. Particle size analysis confirmed that 100% (by weight) of the purified material consisted of particles smaller than 2.0 μm e.s.d.

5.1.2. Sepiolite (SNe-1)

The purification of sepiolite was conducted in a similar way as that for montmorillonite MWy-2, with a few changes.

An amount of 30 grams of brute sepiolite was broken up into small pieces followed by wet grinding with a mortar and pestle. This material was then vigorously mixed overnight with 1.5 litres of deionized water to yield a ~2% suspension. To destroy any insoluble carbonates that may be present as impurities, 1 M HCl was added dropwise under vigorous stirring until the pH of the suspension reached a value of 3.5. As the first portions of the added acid reacted with the carbonates, the pH of the suspension would go up after a couple of minutes; small amounts of HCl solution had to be added repeatedly to keep the pH at the 3.5 value. As soon as the carbonates present in the clay sample were depleted by the reaction with the acid, the pH remained stable at 3.5 for at least 15 minutes, without the need to add more acid.

As reported elsewhere in the literature, care had to be taken to avoid lowering the pH below the 3.5 value, as that could favour the acid attack onto sepiolite which would result in amorphous silica formation. Even exposing the sepiolite to the "safe" acidity level of pH 3.5 was kept to a minimum.

The suspension was then centrifuged using 250 ml centrifuge flasks. After 20 minutes at 4000 rpm, all solid particles previously in suspension were neatly deposited in a well-defined sediment layer at the bottom of the flasks while all soluble species remained dissolved in the supernatant aqueous layer. The clear supernatant solution was discarded. The remaining sediment was redispersed in dilute HCl (pH=3.5) and again centrifuged.

Three such cycles (suspension centrifugation - supernatant discarding - sediment redispersion) were deemed necessary for a complete removal of all carbonates and related products resulted from the reaction of carbonates with acid.

The sediment from the final centrifugation step was added to a 4 litre beaker and redispersed in 3.6 litres of deionized water; this suspension was vigorously stirred for 1 hour. The beaker was then covered and natural sedimentation was allowed to take place, with the goal of collecting as much as possible of the fraction of particles smaller than 0.2 μm e.s.d. (equivalent spherical diameter). After 16 hours of sedimentation time, all particles larger than 0.2 μm e.s.d. should have had settled below 20 cm from the surface, so the top 20 cm portion of the supernatant (containing the finest clay fractions) was siphoned out and collected.

The remaining sediment (still containing a significant amount of small clay particles) was redispersed in water to the 3.6 litre mark then sonified for 10 s and allowed to settle again for 16 hours. The sediment was discarded while the top 20 cm portion of the supernatant from this second sedimentation procedure was collected and combined with the similar fraction from the first sedimentation in a large (6 litre) Erlenmeyer flask. An amount of 250-300 g of solid, reagent grade NaCl was then added to this flask under stirring. This caused the suspended clay particles to flocculate and settle to the bottom of the flask. Also, the large excess of NaCl in solution resulted in a complete replacement (exchange) of all other naturally present cations with Na^+ cation. After standing overnight, two distinct layers could be noticed: a clear supernatant and a grey sediment. The clear supernatant solution was discarded, and the flocculated sediment was collected and placed in dialysis bags. The dialysis bags were then submerged in 10 litres of deionized water

contained in a large tub; the water surrounding the bags was frequently changed with fresh deionized water over the course of 7-14 days.

When the water surrounding the dialysis bags tested negative for Cl^- ions using a saturated $AgNO_3$ solution (meaning that all the excess ionic species had been completely washed away) the contents of the bags were transferred to a thick walled flask and freeze dried under high vacuum. After freeze drying, a fluffy, off-white, pure sepiolite was obtained. Overall, the yield of purified clay was 5-10% starting from the crude sepiolite.

The material thus purified underwent characterization by XRD and particle size analysis. Comparison of the crude and purified samples showed that most of the impurities had been removed through sedimentation and that the amount of sepiolite attacked by the hydrochloric acid was insignificant. Particle size analysis confirmed that 100% (by weight) of the purified material consisted of particles smaller than 2.0 μm e.s.d.

5.2. Pillaring of Montmorillonite Clay

Purified Na^+-M was first exchanged or intercalated with $[Al_{13}]^{7+}$ clusters followed by "pillaring' which was accomplished by calcination at temperatures ranging from 400-500 °C. In order to distinguish between $[Al_{13}]^{7+}$ exchanged or intercalated smectite and $[Al_{13}]^{7+}$ pillared or calcined clay the letters E and P are added to the code in order to specify whether the $[Al_{13}]^{7+}$ -smectite material is respectively exchanged or pillared. For example, Al_{13}M-E denotes montmorillonite which has been exchanged or intercalated with $[Al_{13}]^{7+}$ clusters but not yet calcined, whereas Al_{13}M-P denotes the same material after pillaring or calcination. The $[Al_{13}]^{7+}$ solution used for the exchange of Na^+ with $[Al_{13}]^{7+}$ in

the interlayer space of the smectite is, for historical reasons, called the pillaring solution, and not the exchange solution.

5.2.1 Preparation of Clay Suspensions

A suspension of 10 g of purified Na^+-M in 1.0 L of water was prepared as follows: 10 grams of purified freeze dried material was stirred for at least 24 hours in 1.0 L of water in order to ensure as complete a dispersion as possible.

5.2.2 Preparation of the Stock and Pillaring Solutions

0.5 M NaOH stock solution was prepared by dissolving 20.0 g of fresh NaOH (FW=40.00) pellets in deionized water followed by dilution to 1.00 L. 0.40 M $AlCl_3$ stock solution was prepared by dissolving 96.6 g of $AlCl_3(H_2O)_6$ (Aldrich; FW 241.43) in deionized water and diluting to a total volume of 1.00 L. Both the stock $AlCl_3$ and NaOH solutions were stored in 1.0 L polyethylene bottles.

The pillaring solution was prepared by the slow, dropwise addition (using a 1.0 L dropping funnel) of 0.90 L of 0.50 M NaOH stock solution (450 mmol OH^-), under vigorous magnetic stirring, to 0.50 L of 0.40 M $AlCl_3$ (200 mmol Al^{3+}) which has been diluted to 1.00 L with deionized water in a 4.0 L beaker. The rate of addition of the NaOH solution was approximately 5 mL/min, so the total addition time was about three hours. After addition of NaOH solution, enough deionized water (about 100 mL) was added to the pillaring solution so that the final volume was 2.00 L.

This opalescent hydroxyaluminum solution was then sealed with parafilm and aged under vigorous stirring at room temperature (20 °C) for 24-48 hours, at which time the solution became completely clear. The final OH^-/Al^{3+} ratio of the pillaring solution was 2.25 and the pH was measured to be 4.1. The final concentration of Al^{3+} in the pillaring solution was 0.10 M. Solution state ^{27}Al NMR (Brucker AMX 500; 130.3 MHz; δ (ppm); $Al(NO_3)_3$ reference) confirmed the presence of the $[Al_{13}]^{7+}$ Keggin ion in the pillaring solution. This was seen as a sharp resonance at 63.0 ppm, characteristic of the central aluminum in the $[Al_{13}]^{7+}$ cluster, and has been reported elsewhere (Fu et al., 1991). The octahedrally coordinated aluminums were observed as a broad band centered near 0 ppm.

5.2.3 Exchange Reaction

Under vigorous stirring provided by a high shear mechanical stirrer, 2.00 L of the pillaring solution ($[Al^{3+}]$= 0.10 M; $[OH^-]/[Al^{3+}]$=2.25; 200 mmol Al^{3+}) was added dropwise via a 1.0 L dropping funnel at an addition rate of about 7 mL/min (total addition time = 5 hours) to 1.00 L of a 1.0 % clay suspension (prepared as described in paragraph 5.2.1 above) in a 4.0 L beaker. The final suspension can be described by the following parameters: $[Al^{3+}]_{added}$/(quantity of clay) = 20 mmol/g; $[Al^{3+}]_{added}$ = 0.067 M; final clay content = 0.33 % by weight. Vigorous stirring was necessary, especially at the beginning of the addition, since flocculation was often a problem causing a dramatic increase in the viscosity of the suspension. It has been reported that flocculation interferes with the effective pillaring of smectite clays. Once the addition was complete, the suspension was aged under stirring at room temperature (20 °C) for 24 hours followed by further aging for

24-72 hours without stirring in order to allow for sedimentation of the clay suspension to occur.

The supernatant was then drawn off and the sediment was collected and centrifuged followed by the redispersion in deionized water to a total volume of about 1.50 L. This suspension was then placed in dialysis bags, followed by numerous washings with deionized water to remove all soluble salts and excess $[Al_{13}]^{7+}$ ions. Washing generally involved changing the water of the 8 L wash basin 1-2 times daily. This was repeated until the wash water surrounding the dialysis bag was shown to test negative for Cl^- using an aqueous $AgNO_3$ test reagent. If chloride ion was detectable, one would observe the formation of a fine cloudy white AgCl suspension upon the addition of $AgNO_3$ solution. It normally took anywhere from 2-6 weeks in order for the soluble chloride salts to be completely washed out from sediment within the dialysis bags. Factors which contributed to the speed in which the chloride could be removed included: concentration (viscosity) of the suspension within the dialysis bags, frequency of washing, efficiency of mixing, and the physical condition of the dialysis bags (clogging of pores).

After washing, the suspension was then centrifuged a final time, and the resulting sediment was freeze dried. This procedure involved collecting the sediment, and coating the inner surface of the bottom 2/3 of a 90 mL capacity freeze drying flask (Labconco), followed by carefully freezing the paste by rotating the flask at an angle in a dry ice/acetone cold bath (temperature = -78 °C). Care was taken not to freeze the paste as a mass at the bottom of the flask, or else the expansion caused by the water freezing could break the glass flask. Once the paste was completely frozen, the flask was immediately placed under high vacuum (5-10 mTorr) for 2-3 days, upon which time freeze-drying was

complete, resulting in a fluffy $[Al_{13}]^{7+}$ exchanged smectite material (Al_{13}-ME). This material was then collected, weighted, characterized by XRD and TGA, and stored in sealed glass jars. Preparation by this procedure typically resulted in 11-12 g of $[Al_{13}]^{7+}$ exchanged smectite.

5.2.4 Calcination

The $[Al_{13}]^{7+}$ exchanged smectites were calcined by heating the clays up to 500 °C at a rate of 1-3 °C/min, and holding at 500 °C for three hours, before cooling back down to 30 °C. The sample weights were all measured before and after calcination, indicating weight losses ranging from 7-12 %. Both the uncalcined (Al_{13}-ME) and the calcined pillared smectite (Al_{13}-MP) were characterized by XRD, and stored in glass jars. The measured basal spacing (d_{001}) of this materials are shown in Table 5.1.

Table 5.1. Basal Spacing of Pillared Montmorillonite.

Sample	Temperature (°C)	d_{001} (Å)
Al_{13}-ME	25	18.3
Al_{13}-MP	500	12.9

5.3 Preparation of Clay/Boehmite Composite Membranes

5.3.1 Preparation of 1.0 M Boehmite Stock Solution

The boehmite stock solution which was used in the preparation of both the unsupported and supported membranes was prepared following previously reported literature methods (Lao et al., 1994, Uhlhorn et al.,1992) . An amount of 128 g (0.51 moles) of aluminum tri-*sec*-butoxide (Aldrich; 97%; FW 246.33) was added dropwise from a 1.0 L dropping funnel into 750 ml of deionized water in a 2.0 L beaker under vigorous stirring. The temperature of the water solution in the 2.0 L beaker was maintained at a temperature between 80 and 90°C using a hotplate. The total addition time was 75 minutes at time a viscous white suspension could be observed.

To this heated mixture, 3.4 g of concentrated nitric acid (70% by weight; FW 63.01; 38 mmol) was added to peptize (stabilize) the sol. The quantity of acid was chosen such that the ratio $[HNO_3]/[Al^{3+}]$ was 0.07 since this was reported in the literature (Cho et al., 1995) as being the optimum amount of acid additive to prepare a stable boehmite sol with a particle size distribution centred around a diameter of about 55 nm with a diameter range between 8 and 400 nm. This sol was also reported (Cho et al., 1995) to be stable over time, with the mean particle size increasing only slightly after 23 days.

The sol was boiled in an open atmosphere in order to reduce the volume to 0.5 L. This was then transferred into a 1.0 L round bottom flask, fitted with a condenser and refluxed for 17 hours, resulting in a translucent 1.0 M boehmite sol. The density of this boehmite sol was measured to be 1.048 g/cm^3 and was found to contain 63 mg of solid material per 1.0 g of solution, which is in agreement with what one might expect for a 1 M

AlOOH solution. This solution was placed in a sealed polyethylene bottle for storage and was used in the preparation of all membranes requiring boehmite sol.

5.3.2 Unsupported Membranes

5.3.2.1 Unsupported Montmorillonite/Boehmite Composite Membranes for Gas Permeation Experiments

The method used in the preparation of unsupported montmorillonite membranes involved an $[Al_{13}]^{7+}$ exchanged montmorillonite (Al_{13}-ME) which had not yet been calcined. Calculated amounts of this purified clay, which had been stored in glass jars for variable times without calcination, were dispersed by mixing in a given amount of deionized water in a glass vial. When a homogeneous mixture was obtained, a calculated amount of boehmite sol from the 1.0 M stock solution was added and magnetically stirred for a given amount of time, followed by casting onto a plastic petri dish (surface area of 55.4 cm^2).

The quantities of boehmite, pillared clay and water were calculated such that the total dry weight of both the pillared clay and the boehmite was 1.0 g, dispersed in enough water to give a total mass of 15-20 g. The percentage of clay as the total dry weight of the clay/boehmite mixture is indicated in the membrane code description (Table 6.1). For example, membrane UM 06 of type Al_{13}M-90-Al indicates that this is unsupported (U) montmorillonite (M) membrane number 6 and is made up of a mixture of 90% Al_{13}-ME and 10% boehmite (before calcination). After calcination, Al_{13}-ME turns into Al_{13}-MP so that the symbol Al_{13}-M was used in the membrane code for simplicity; also the boehmite

turns, upon calcination, into aluminum oxide Al_2O_3 (alumina), hence the symbol Al at the end of a membrane code. The thickness of the unsupported membranes could be crudely controlled by controlling the amount of clay and boehmite deposited per unit area of the petri dish. The thickness of the membranes was always measured using a Mitutuyo digital micrometer. To compensate for the minute deviations from absolute flatness (which "inflate" the thickness measurements), the values read from the digital display were always rounded down to the nearest multiple of 5 μm (e.g. a thickness of 104 μm read from the Mitutuyo digital display is reported as 100 μm).

Drying of the membranes had to be done slowly and carefully in order to prevent cracking. This was done in one of two ways.

The first involved covering the petri dish containing the clay / boehmite sol with parafilm, perforating the parafilm with numerous small holes and then allowing the suspension to dry in ambient conditions, thus forming the air dried membrane. The perforated parafilm cover served to slow the drying process.

The second drying method involved placing the open petri dish and contents in an enclosed bell jar containing a small quantity of Drierite® brand desiccant (anhydrous calcium sulphate) at the bottom. The drying rate could be controlled to some extent by the judicious addition of small quantities of fresh Drierite®. Drying of the membranes in these two manners typically took anywhere from two to six days, at which time the membranes often curled off the plastic petri dish, or could easily be pealed off. A portion of this air-dried composite clay / boehmite membrane was often broken off and analysed by TGA and XRD before calcination.

The remaining portion of the membrane was then weighed and carefully placed in a porcelain crucible and calcined in a programmable temperature oven. The calcination

program involved ramping up at a rate of 1-3°C / minute from room temperature to 450-500°C, maintaining this maximum temperature for three hours, followed by cooling at a controlled rate of 3°C / minute. The membranes were then removed from the oven, weighed, placed in labelled petri dishes and stored in desiccator until membrane mounting.

5.3.2.2 Unsupported Sepiolite/Boehmite Composite Membranes for Gas Permeation and Ultrafiltration Experiments

Sepiolite/boehmite composite membranes were made by the procedure described as follows. Purified and freeze dried Sepiolite from Nevada was mixed overnight with distilled water and a certain amount of boehmite sol, then sonified for about 10 minutes; the viscous suspension was then filtered through a 100 μm pore size ceramic filter and poured into plastic Petri dishes. The quantities of boehmite, sepiolite and water were calculated such that the total dry weight of clay and boehmite together was 1.1 g , dispersed in enough water to give a total mass of 70-75 g. The dishes were left uncovered in open atmosphere (under a small canopy to protect against dust settling onto dishes) for 3-4 days after which time a dry flat sheet of material could be easily peeled off the Petri dish.

These sheets were then weighed, carefully placed in a porcelain crucible and calcined in a programmable temperature oven. The calcination program involved ramping up at a rate of 1-3°C / minute from room temperature to 450-770°C, maintaining this maximum temperature for one hour, followed by cooling at a controlled rate of 3°C / minute. The membranes were then removed from the oven, weighed, placed in labelled petri dishes and stored in desiccator until membrane mounting. The resulting membranes were generally flat and about 250 μm thick. The thickness of the membranes was always

measured using a Mitutuyo digital micrometer. To compensate for the minute deviations from absolute flatness (which "inflate" the thickness measurements), the values read from the digital display were always rounded down to the nearest multiple of 10 μm (e.g. a thickness of 259 μm read from the Mitutuyo digital display is reported as 250 μm).

5.3.3 Supported Montmorillonite/Boehmite CompositeMembranes for Gas Permeation Experiments

Supported membranes were prepared in much the same way as the unsupported membranes, using $[Al_{13}]^{7+}$ exchanged (Al_{13}-ME) clay. The main differences were that thinner coatings were used and that the membranes were coated on porous supports instead of on plastic petri dishes. All of the supported membranes which were prepared in this project are described in Table 6.9.

The clay / boehmite mixture was prepared in the same way as for the unsupported membranes, except that smaller quantities were needed since the coated surface area of the disks and tubes was smaller than the 55.4 cm^2 of a petri dish; also thinner coating layers were sought. Usually, when the clay / boehmite / water mixture was prepared for the unsupported membranes, an excess was prepared and a portion of this was used in the preparation of supported membranes. This was usually diluted accordingly with deionized water to give a suspension with a known concentration of clay/boehmite in water (anywhere from 0.1% to 6.7% total solids in water, by weight). Controlling exactly the amount of solids in the coating solution allowed the coating of a controlled layer thickness of boehmite/clay onto the supports.

The supports (both disks and tubes, described in detail in section 4.1) were calcined by their manufacturer at temperatures above 1200°C; in the laboratory, they were normally not pre-treated in any way, except for washing, drying and storage in a desiccator (over Drierite®) prior to coating. Some supports were smoothed by grinding one side (the side to be coated) with a 600 grit sandpaper. Few alumina supports were coated first with boehmite sol and then with the clay-boehmite mixture.

The coating of the disks was done by pipetting a measured quantity of the clay/boehmite/water suspension and carefully dropping the suspension onto the upper surface of the disk, covering the entire surface as uniformly as possible. The suspension was then allowed to dry in a desiccator over Drierite®, leaving behind a clay-boehmite coating on the disk. The disk was normally dry after sitting overnight for 16 hours in the dessicator. The coated disk was then placed in a digitally programmable oven and calcined at 450-500°C, as described for the unsupported membranes. When more coatings were required, this entire procedure (pipetting, drying and calcination) was repeated until the desired cumulative thickness and/or number of layers were achieved. After each calcination step, the thickness of the whole membrane (support + coated layers) was measured with a Mitutuyo digital micrometer and the thickness of the most recently coated layer was calculated as the difference between the total thickness before and after the new layer.

Coating of the tubes was performed using a dip coating technique. The supports were immersed vertically in the clay/boehmite suspension for 30 seconds prior to slow removal and drying. When fully dipped into the coating suspension, the alumina tubes had one end plugged and the other end attached to a long piece of rubber hose (to prevent coating the inside surface of the tubular support, without creating air pockets inside). When

more coatings were required, this entire procedure (dip-coating, drying and calcination) was repeated until the desired cumulative thickness and/or number of layers were achieved. After each calcination step, the thickness of the whole membrane (support + coated layers) was measured with a Mitutuyo digital micrometer and the thickness of the most recently coated layer was calculated as the difference between the total thickness before and after the new layer.

5.4 Membrane Mounting

Two types of heat resistant glues were used to mount the membranes onto aluminum foil supports. One was a silicone rubber sealant (Bostick RTV Silicone Sealant; Bostick, Middleton, MA 01949) which is based on crosslinked silicone rubber, and the other is an epoxy glue (Scotch-Weld Epoxy Adhesive 2214 Hi-Temp; 3M, St. Paul, MN 55144).

5.4.1 Unsupported Membranes

Circular pieces of 1-6 cm^2 surface area were cut off the flattest areas of the calcined unsupported membranes and mounted as shown in Figure 5.1. The membranes were glued either with silicone rubber or with epoxy, to an aluminum foil backing (thickness 150 μm, diameter 8 cm) which has been perforated in the central area where the membrane sits. For cushioning, a layer of filter paper or porous soft cellulose plaster was placed between the membrane and aluminum foil.

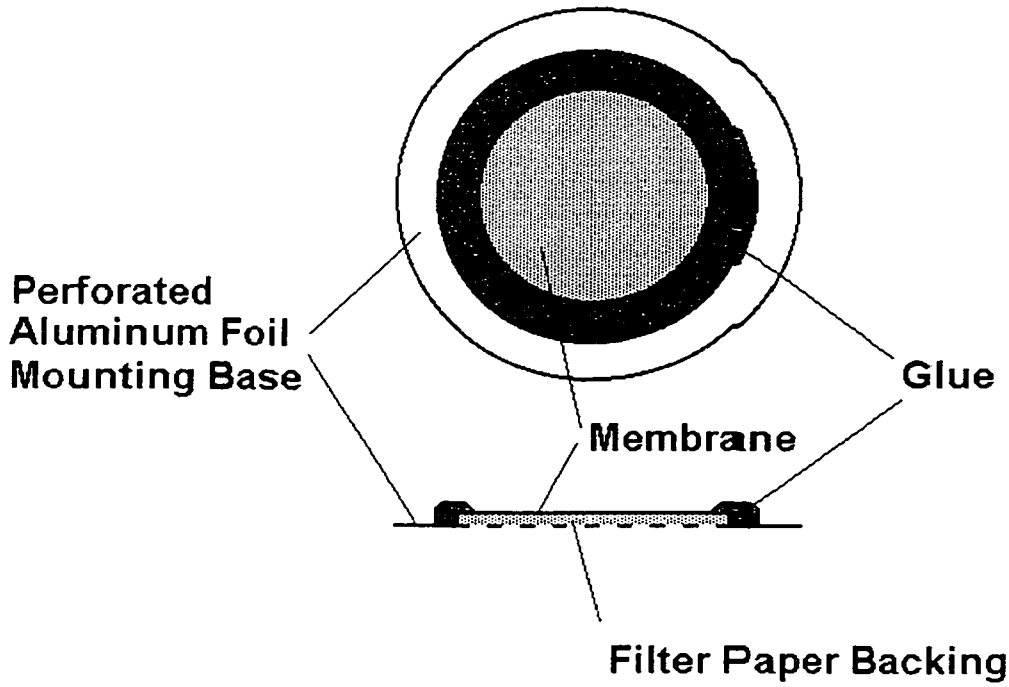

Figure 5.1. Unsupported Membranes Mounted on Aluminum Foil Base.

5.4.2 Supported Membranes

The coated Hytrex alumina discs were glued, either with silicone rubber or with epoxy, directly onto aluminum foil backings similar to those described above, only instead of the membrane resting on a perforated backing, it rested on a 7 cm^2 area portion which had been cut out for this purpose (Figure 5.2).

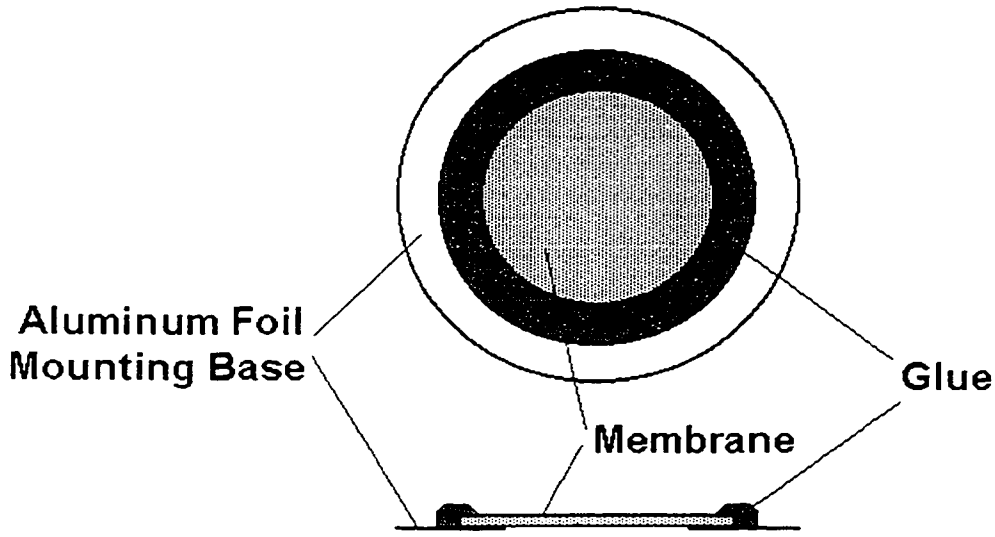

Figure 5.2. Disk-supported Membranes Mounted on Aluminum Foil Base.

The coated Hytrex alumina tubular supports had one end plugged by an impermeable disk, while the other end was glued with silicone rubber directly onto an aluminum foil base similar to those described above (Figure 5.3).

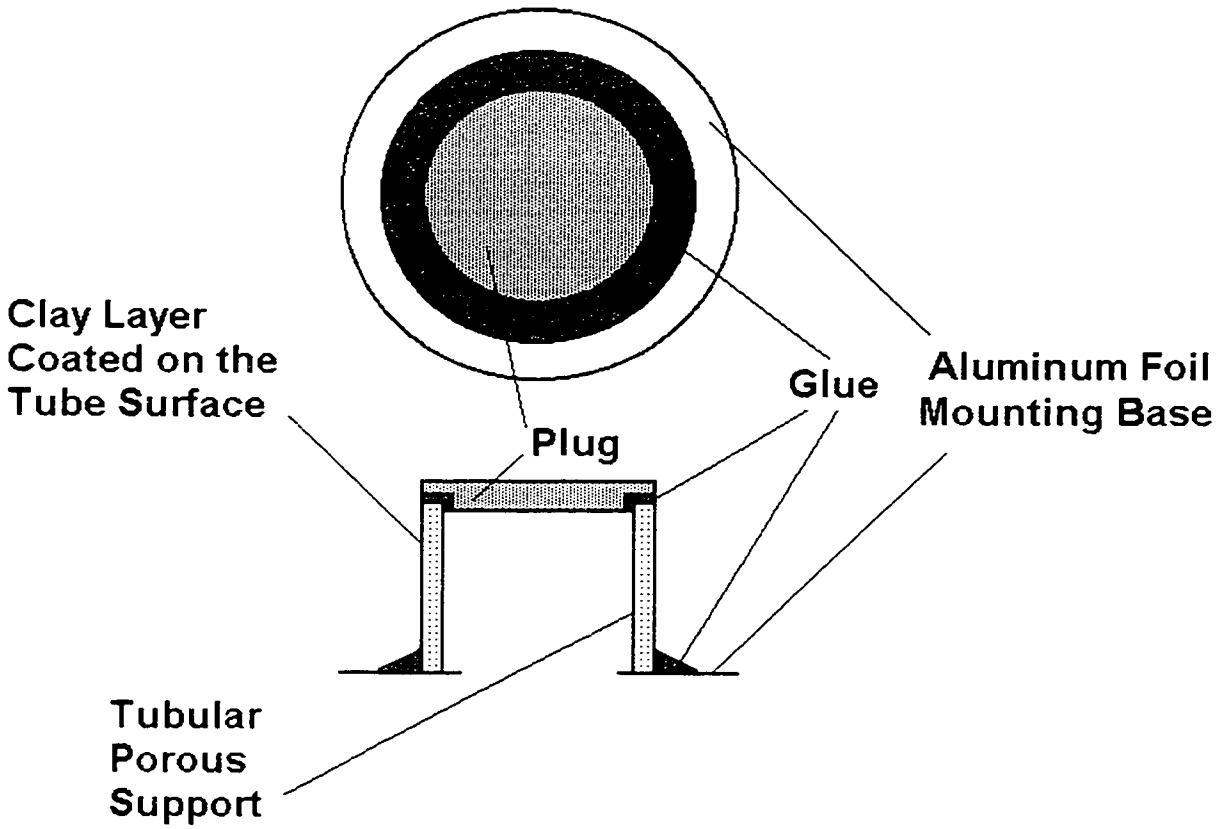

Figure 5.3. Tube-supported Membranes Mounted on Aluminum Foil Base.

5.5 Membrane Testing

5.5.1 Experimental Setup

5.5.1.1 Gas permeation

The membranes were tested for gas permeation using the experimental setup described in Figure 5.4.

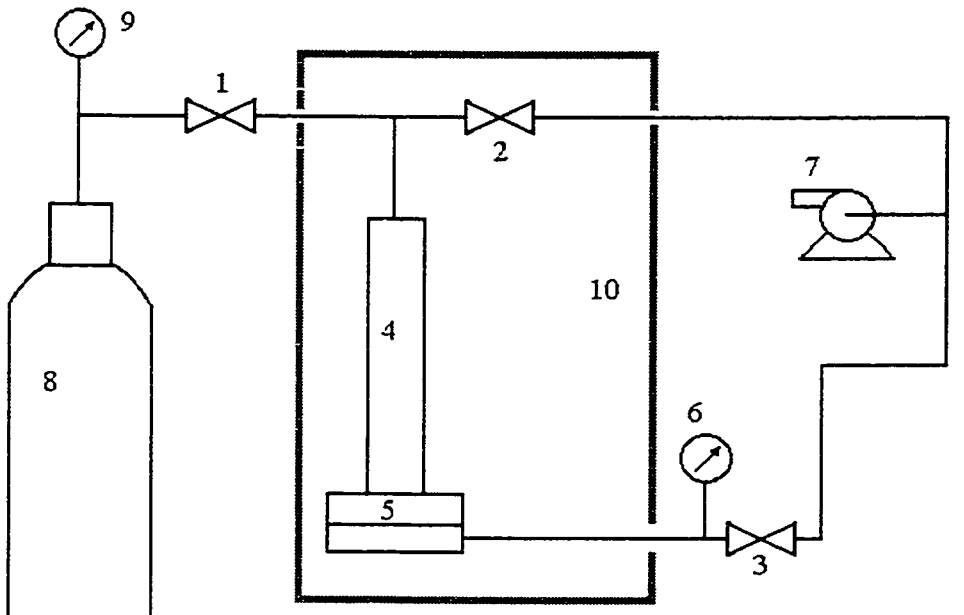

1-3 Valves
4 Permeation Cell
5 Membrane
6 Vacuum Gauge
7 Vacuum Pump
8 Compressed Gas Cylinder
9 Pressure Gauge
10 Programmable Temperature Oven

Figure 5.4. Experimental Setup for Gas Permeation.

Basically, this experimental set up is a dead end (static)configuration; since only small amounts of permeate were collected, the transmembrane pressure was assumed to remain constant during the experiments. The testing procedure is described as follows (refer to Figure 5.4).

a) The permeation cell containing the membrane to be tested was placed inside the oven, all connections were made and the oven was heated to the prescribed temperature.

b) Both sides (permeate side and feed side) were evacuated down to a residual pressure of 1 mbar (absolute) for 3 hours.

c) By closing valve 2 and opening valve 1, gas under a set pressure was applied to the feed side.

d) Permeate side was kept under vacuum for ½ hour until permeation reached steady state.

e) By closing valve 3, a constant volume permeate chamber was created (chamber volume = 23.38 mL). The increase in pressure in this chamber (as shown by the pressure gauge 9) was monitored against time and was used to calculate the permeation rate. The initial pressure in the permeation chamber was 1 mbar and the final reading was always bellow 50 mbar; at these very low pressures, the deviation from ideality of all gases used was assumed to be negligible and the ideal gas law was used to translate the pressure into number of moles. Permeabilities were then calculated by the Eq. 1 (in Chapter 2).

5.5.1.2 Ultrafiltration Experiments

The membranes were tested in ultrafiltration experiments using the experimental setup described in Figure 5.5. Ultrafiltration experiments were done in dead end stirred cell configuration; since only small amounts of permeate were collected, the feed concentration was assumed to remain constant during the experiments.

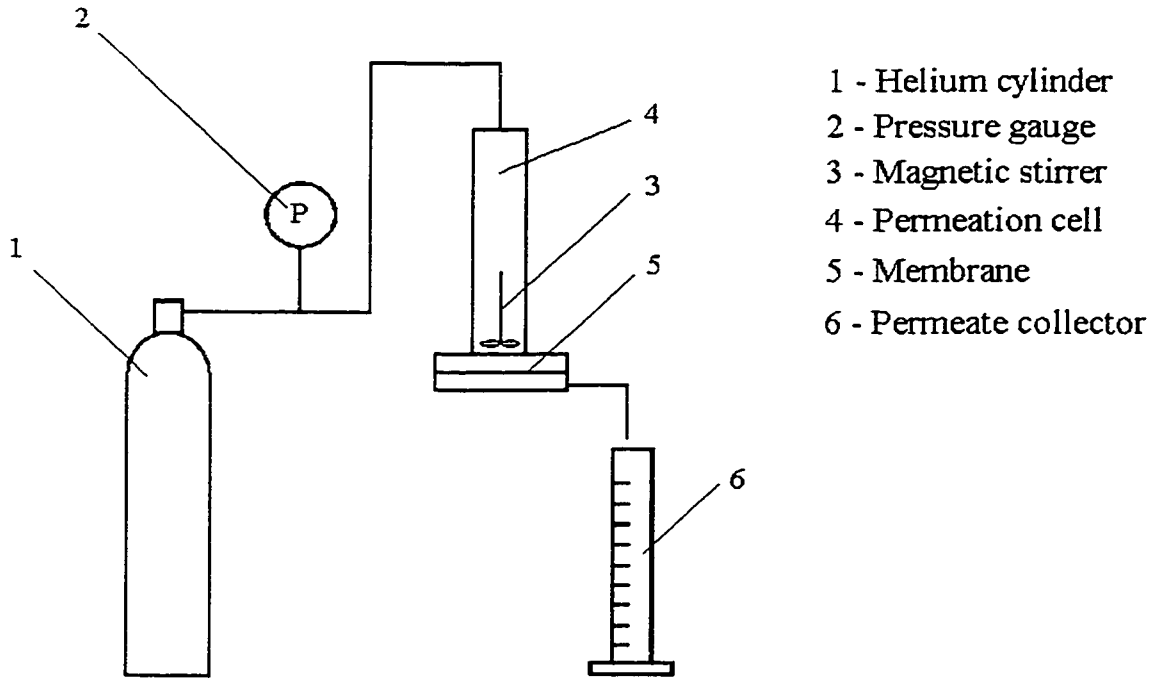

Figure 5.5. Experimental Setup for Ultrafiltration.

The testing procedure was as follows (refer to Figure 5.5):

a) The permeation cell containing the membrane to be tested was filled with the feed solution (492 ml) and the membrane was kept for 12 hours in contact with the feed under slow magnetic stirring (to allow for adsorption/absorption phenomena to reach equilibrium and not interfere with the ultrafiltration experiment). Concentration of the feed solutions was kept constant at 100 ppm for all permeation experiments and it was verified by TOC analysis.

b) The permeation cell containing the membrane to be tested was emptied of liquid then refilled with fresh feed solution and the connection was made to the compressed helium cylinder. Helium pressure was adjusted to the preset value and magnetic stirring was increased to medium speed. Four testing pressures (30 psig, 50 psig, 70 psig and 90 psig) were used and the temperature was always room temperature (20-24 °C).

c) Permeate was collected in a waste bottle for the first 30 minutes (enough to collect 5-10 ml), after which it was assumed that steady state was reached.

d) Permeate was collected in a graduated cylinder; the time required to collect 10 ml of permeate was recorded and the permeate was sent to TOC analysis.

e) The procedure mentioned in the paragraph d) above was repeated three times for each membrane; recorded times and TOC analysis results were then averaged. All volumetric flux data was corrected to 25 °C. More details on the processing of TOC results into separation data are given in section 2.2.

Chapter 6. RESULTS AND DISCUSSIONS

6.1 Unsupported Montmorillonite/Boehmite Composite Membranes-Results of Gas Separation Experiments

The following types of montmorillonite/boehmite composite membranes were cast and calcined as described in the experimental section:

100% Al_{13}-pillared Montmorillonite (Al_{13}M 100)

60% Al_{13}-pillared Montmorillonite – 40% boehmite (Al_{13}M-60-Al)

90% Al_{13}-pillared Montmorillonite – 10% boehmite (Al_{13}M-90-Al)

100% boehmite (AlOOH 100)

All membranes were quite wavy after drying and maintained their wavy shape after calcination; some cracked during the drying period, none cracked during the calcination. A more detailed description of montmorillonite unsupported membranes is given in Table 6.1.

Table 6.1. Description of Unsupported Montmorillonite Membranes.

Membrane code	Membrane type	Thickness (μm)	Calcination Temp.	Description
UM 01	$Al_{13}M$ 100	100	500 °C	Soft, many cracks
UM 02	$Al_{13}M$ 100	100	500 °C	Soft, many cracks
UM 03	$Al_{13}M$-60-Al	100	500 °C	Good appearance, wavy
UM 04	$Al_{13}M$-60-Al	100	500 °C	Good appearance, wavy
UM 05	$Al_{13}M$-60-Al	100	500 °C	Good, wavy, one small crack
UM 06	$Al_{13}M$-90-Al	100	500 °C	Good, wavy, some cracks
UM 07	$Al_{13}M$-90-Al	100	500 °C	Wavy, cracks
UM 08	AlOOH 100	100	500 °C	Brittle, many cracks
UM 09	AlOOH 100	100	500 °C	Brittle, many cracks

Membranes UM 01, UM 02, UM 07, UM 08 and UM 09 could not be tested; because of their brittle nature they broke during attempts to mount them on the aluminum foil backing. It was somehow expected that UM 01 and UM 02 (made of pure pillared clay without any binder at all) would form less cohesive films; also membranes made of pure boehmite (UM 08 and UM 09) are reported in the literature to crack upon drying, unless some special additives and drying conditions are employed in their manufacture (Yang et al., 1996; Reed, 1989).

All other membranes were also fragile and required extreme care in handling and mounting but at least one small (2-6 cm^2) portion from each membrane was successfully tested for gas permeation.

Before an actual permeation measurement of any membrane, a second membrane (cut from the same coupon of material as the membrane whose permeation was to be measured) was always tested in a similar set-up, at the same temperature and a pressure that exceeded by 25 psia the intended testing pressure of the first membrane. It was found this way that most membranes would break at feed pressures above 75 psig (with the permeate side under full vacuum) which lead to the decision to limit all gas permeation experiments to 50 psig feed pressure. The results are shown in Table 6.2 through Table 6.6.

Table 6.2. Results of the Pure Gas Permeation Experiments with Unsupported Membrane UM 03 (Al_{13}M-60-Al).

Temperature °C	Helium Permeability (Barrer)	Nitrogen Permeability (Barrer)	Permeability Ratio
160	233	1.31	171
180	242	2.08	116.3

Table 6.3. Results of the Pure Gas Permeation Experiments with Unsupported Membrane UM 04 (Al_{13}M-60-Al).

Temperature °C	Helium Permeability (Barrer)	Nitrogen Permeability (Barrer)	Permeability Ratio
140	32	0.15	216
160	45	0.26	171
180	58	0.35	166

Table 6.4. Results of the Pure Gas Permeation Experiments With Unsupported Membrane UM 04 (Al_{13}M-60-Al).

Temperature °C	Hydrogen Permeability (Barrer)	Propane Permeability (Barrer)	Permeability Ratio
140	25	0.11	236
160	33	0.18	184
180	45	0.26	169

Table 6.5. Results of the Pure Gas Permeation Experiments With Unsupported Membrane UM 05 (Al_{13}M-60-Al).

Temperature °C	Helium Permeability (Barrer)	Nitrogen Permeability (Barrer)	Permeability Ratio
140	41	0.22	186
160	53	0.36	147

Table 6.6. Results of the Pure Gas Permeation Experiments With Unsupported Membrane UM 06 (Al_{13}M-90-Al).

Temperature °C	Helium Permeability (Barrer)	Nitrogen Permeability (Barrer)	Permeability Ratio
140	3.2	0.05	64
160	4.3	0.09	48
180	5.1	-	-

As it can be seen from the experimental results, all membranes that could be tested exhibited different permeation rates for different gases. While no mixtures of gases were tested, pure gas permeability is, quite often, a fair indicator of the separation factors that can be expected from these membranes when exposed to a mixed feed. The 60% montmorillonite membranes (UM 03, 04, 05) performed best while the 90% montmorillonite membranes showed less permselectivity (in part due, maybe, to their structural integrity problems).

The results obtained with the membrane UM 04 (the most robust one) could be used in an attempt to explain the nature of the separation mechanism. A full set of 4 gases (helium, hydrogen, nitrogen and propane) could be tested at three different temperatures on this membrane. At any temperature, the permeabilities of the four gases mentioned above are in an inverse relationship with their molecular size (kinetic diameter), shown in Table 6.7. This is a strong argument for a molecular sieving mechanism of transport. Inevitably, the existence of some defects and larger pores makes the molecular sieving to be imperfect, allowing some Knudsen and maybe Poiseuille flow to take place.

Table 6.7. Kinetic Diameter of Various Gas Molecules.

Molecule	**Kinetic Diameter (Å)**
He	2.6
H_2	2.89
H_2O	2.65
NH_3	2.6
N_2	3.64
CO_2	3.3
CH_4	3.8
propane	4.3

For comparison, selected values of permeability reported in the literature on different types of inorganic membranes are shown in Table 6.8. It can be seen that the pillared montmorillonite membranes compare favourably with other inorganic membranes, displaying either higher permeability or higher selectivity than most other membranes.

Table 6.8. Selected Inorganic Membrane Performance Data from the Literature.

Membrane	**Permeability (barrer)**	**T (°C)**	**Permeability ratio**	**Reference**
Pd-Ag alloy/alumina	H_2 = 112 He = 53.8	250	H_2/N_2 = 5.7	Jarayaman and Liu, 1995
Hollow fibre silica	H_2 = 734	150	H_2/N_2 = 103	Hassan et al.,1995
Silica on gamma alumina support	He = 2198	25	He /N_2 = 1.3	Raman and Brinker, 1995
Silica on gamma alumina support	He = 13.1	25	He /N_2 = 14.4	Raman and Brinker, 1995
Silica on gamma alumina tube	He = 4779	300	He /N_2 = 36	Wu et al.,1994
Carbon Molecular Sieve	H_2 = 5078	25	H_2/N_2 = 23.6	Shusen et al.,1995

Despite the good theoretical separation factors exhibited, unsupported montmorillonite membranes were found to suffer from a lack of practicality, due to their fragility, low permeation flux, irregular shape and variations in performance from batch to batch. This was the main reason for discontinuing further investigations on unsupported membranes and focusing on attempts to build supported membranes using the same material that performed best in unsupported membranes: 60% pillared montmorillonite and 40% boehmite.

The rationale was that a better membrane could be made by depositing a much thinner layer of this permselective material on a commercially available porous support, with the assumption that the selectivity would not be significantly reduced by the reduction in layer thickness. For example, reducing the thickness of the permselective layer from 100 μm (as in the unsupported membranes discussed above) to 1-10 μm could theoretically boost throughput by 1 to 2 orders of magnitude, which would be a major achievement. Also, the use of robust, easily available, porous supports, in a variety of shapes (tubes, disks, hollow fibers), would add safety, convenience, simplicity and flexibility to module building, possibly unlocking the true potential for large scale applications (including high-temperature membrane reactors).

6.2 Supported Montmorillonite/Boehmite Membranes-Results of Gas Separation Experiments

Since 60% montmorillonite – 40% boehmite was the composition that gave the best results with unsupported membranes, only this material was used in all attempts at coating the supports with a thin permselective layer. Unfortunately, all attempts to obtain a satisfactory supported membrane failed. Table 6.9 contains descriptions of all supported membranes built for this project. All membranes in Table 6.9 were calcined at 500 °C and all showed high individual gas permeabilities and low permeability ratios between helium and nitrogen at room temperature (less than 2.1, comparable to the uncoated supports).

Table 6.9. Supported Montmorillonite/Boehmite Membranes (Al_{13}M-60-Al)

Membrane code	Support (pore diameter/shape)	Deposited layer(s), thickness of each layer, material, etc.	Physical appearance
SM 01	0.2 μm disk	One 0.5 μm layer of clay/boehmite	Good
SM 02	0.2 μm disk	One 1.0 μm layer of clay/boehmite	good
SM 03	0.2 μm disk	One 2 μm layer of clay/boehmite	good
SM 04	0.2 μm disk	One 5 μm layer of clay/boehmite	cracks
SM 05	0.2 μm disk	One 10 μm layer of clay/boehmite	cracks
SM 06	0.2 μm disk	One 1.0 μm layer of pure boehmite followed by one 5 μm layer of clay/boehmite mixture	cracks
SM 07	0.2 μm disk	Two 1.0 μm layers of pure boehmite followed by one 5 μm layer of clay/boehmite mixture	cracks
SM 08	0.2 μm disk	Three 1.0 μm layers of pure boehmite followed by one 5 μm layer of clay/boehmite mixture	cracks
SM 09	0.2 μm disk	Four 1.0 μm layers of pure boehmite followed by one 5 μm layer of clay/boehmite mixture	cracks
SM 10	0.2 μm disk	Five 1.0 μm layers of pure boehmite followed by one 5 μm layer of clay/boehmite mixture	cracks
SM 11	0.2 μm disk	One 1.0 μm layer of pure boehmite followed by one 0.5 μm layer of clay/boehmite mixture	good
SM 12	0.2 μm disk	One 1.0 μm layer of pure boehmite followed by two 0.5 μm layers of clay/boehmite mixture	good
SM 13	0.2 μm disk	One 1.0 μm layer of pure boehmite followed by three 0.5 μm layers of clay/boehmite mixture	good
SM 14	0.2 μm disk	One 1.0 μm layer of pure boehmite followed by four 0.5 μm layers of clay/boehmite mixture	good

Table 6.9. Supported Montmorillonite/Boehmite Membranes (Al_{13}M-60-Al)

Membrane code	Support (pore diameter/shape)	Deposited layer(s)	Physical appearance
SM 15	0.2 μm disk	One 1.0 μm layer of pure boehmite followed by five 0.5 μm layers of clay/boehmite mixture	good
SM 16	0.2 μm disk	One 1.0 μm layer of pure boehmite followed by six 0.5 μm layers of clay/boehmite mixture	good
SM 17	0.2 μm disk	One 1.0 μm layer of pure boehmite followed by seven 0.5 μm layers of clay/boehmite mixture	good
SM 18	0.2 μm disk	One 1.0 μm layer of pure boehmite followed by eight 0.5 μm layers of clay/boehmite mixture	cracks
SM 19	0.1 μm tube	One 1.0 μm layer of clay/boehmite	good
SM 20	0.1 μm tube	One 5.0 μm layer of clay/boehmite	cracks
SM 21	0.1 μm tube	One 10 μm layer of clay/boehmite	cracks
SM 22	0.1 μm tube	One 1.0 μm layer of pure boehmite followed by one 5 μm layer of clay/boehmite mixture	cracks
SM 23	0.1 μm tube	One 1.0 μm layer of pure boehmite followed by two 0.5 μm layers of clay/boehmite mixture	good
SM 24	0.1 μm tube	One 1.0 μm layer of pure boehmite followed by six 0.5 μm layers of clay/boehmite mixture	good
SM 25	0.3 μm tube	One 1.0 μm layer of clay/boehmite	good
SM 26	0.3 μm tube	One 5.0 μm layer of clay/boehmite	good
SM 27	0.3 μm tube	One 10 μm layer of clay/boehmite	cracks
SM 28	0.3 μm tube	One 1.0 μm layer of pure boehmite followed by one 5 μm layer of clay/boehmite mixture	cracks

Table 6.9 (continued). Supported montmorillonite/boehmite membranes (Al_{13}M-60-Al)

Membrane code	Support (pore diameter/shape)	Deposited layer(s)	Physical appearance
SM 29	0.3 μm tube	One 1.0 μm layer of pure boehmite followed by two 0.5 μm layers of clay/boehmite mixture	good
SM 30	0.3 μm tube	One 1.0 μm layer of pure boehmite followed by six 0.5 μm layers of clay/boehmite mixture	good
SM 31	0.7 μm tube	One 1.0 μm layer of clay/boehmite	good
SM 32	0.7 μm tube	One 5.0 μm layer of clay/boehmite	good
SM 33	0.7 μm tube	One 10 μm layer of clay/boehmite	good
SM 34	0.7 μm tube	One 1.0 μm layer of pure boehmite followed by one 5 μm layer of clay/boehmite mixture	cracks
SM 35	0.7 μm tube	One 1.0 μm layer of pure boehmite followed by two 0.5 μm layers of clay/boehmite mixture	good
SM 36	0.7 μm tube	One 1.0 μm layer of pure boehmite followed by six 0.5 μm layers of clay/boehmite mixture	good
SM 37	1.0 μm tube	One 1.0 μm layer of clay/boehmite	good
SM 38	1.0 μm tube	One 5.0 μm layer of clay/boehmite	good
SM 39	1.0 μm tube	One 10 μm layer of clay/boehmite	good
SM 40	1.0 μm tube	One 1.0 μm layer of pure boehmite followed by one 5 μm layer of clay/boehmite mixture	good
SM 41	1.0 μm tube	One 1.0 μm layer of pure boehmite followed by two 0.5 μm layers of clay/boehmite mixture	good
SM 42	1.0 μm tube	One 1.0 μm layer of pure boehmite followed by six 0.5 μm layers of clay/boehmite mixture	good

Table 6.10 Gas Permeation Rates for Supported Montmorillonite/Boehmite Membranes (Al_{13}M-60-Al)

Membrane	Nitrogen Permeance mol/m^{2}sPa	Membrane	Nitrogen Permeance mol/m^{2}sPa	Membrane	Nitrogen Permeance mol/m^{2}sPa
SM 01	2.8 E-06	SM 15	8.4 E-07	SM 29	6.7 E-07
SM 02	2.5 E-06	SM 16	8.3 E-07	SM 30	2.3 E-07
SM 03	2.1 E-06	SM 17	8.3 E-07	SM 31	2.9 E-05
SM 04	2.0 E-06	SM 18	8.0 E-07	SM 32	8.8 E-06
SM 05	1.9 E-06	SM 19	8.1 E-07	SM 33	2.1 E-06
SM 06	6.3 E-07	SM 20	7.5 E-07	SM 34	3.9 E-06
SM 07	5.0 E-07	SM 21	7.4 E-07	SM 35	0.6 E-06
SM 08	3.8 E-07	SM 22	9.3 E-08	SM 36	9.7 E-07
SM 09	2.9 E-07	SM 23	9.6 E-08	SM 37	5.7 E-05
SM 10	2.4 E-07	SM 24	8.2 E-08	SM 38	2.5 E-05
SM 11	9.8 E-07	SM 25	2.9 E-06	SM 39	1.6 E-06
SM 12	9.2 E-07	SM 26	1.2 E-06	SM 40	0.6 E-06
SM 13	8.8 E-07	SM 27	1.1 E-06	SM 41	0.8 E-06
SM 14	8.7 E-07	SM 28	9.7 E-07	SM 42	9.9 E-07

Note: 1 mol/m^{2}sPa = 2.987x10^{13} cm^3(STP)/cm^2 s cmHg = 2.987x10^{13} Barrer/cm

Several trends can be noticed from the data in Table 6.9 and 6.10. One is that multiple thin coatings seem to offer a better coverage than one thick coating (e.g. SM40 vs. SM42. SM34 vs. SM36). Also an intermediate layer of boehmite between the support and

the coated layers reduces the incidence of cracks. Lastly, it seems that supports with larger pore sizes tend to impart better integrity to membranes (less cracks, lower flow rates).

Even though these trends apply only to the apparent integrity of the deposited clay layers (and not to the separation performance itself that was nonexistent for all membranes), they could still be of some value for future work on this topic, since a crack free permselective layer and good adhesion to support are prerequisites for any supported membrane. Cracks are a result of mechanical stresses that occur during drying and calcination, when the gel structure undergoes dramatic changes and sometimes collapses. Interaction and chemical compatibility between the gel layer and the support plays an important role, together with the relative position of the coated layer versus the support (e.g. inside the pores or on the surface of the support) and the rate of drying. Ideally, an optimum set of conditions should exist for each pair of support-coating layer and these optimum conditions could not be found for the membranes described above.

6.3 Unsupported Sepiolite/Boehmite Composite Membranes

The following types of sepiolite unsupported membranes were cast and calcined as described in the experimental section:

100% sepiolite

60% sepiolite – 40% boehmite

90% sepiolite – 10% boehmite

All membranes were flat after drying and maintained their shape after calcination; the membranes made of 90% sepiolite – 10% boehmite cracked during the drying period, none cracked during the calcination. A more detailed description of sepiolite unsupported membranes is given in Table 6.11.

Table 6.11. Sepiolite Unsupported Membranes

Membrane code	Membrane type	Thickness (μm)	Calcination Temp.	Physical appearance
US 10	100% sepiolite	250	500 °C	good, flat
US 11	100% sepiolite	250	500 °C	good, flat
US 12	100% sepiolite	250	765 °C	good, flat
US 13	100% sepiolite	250	765 °C	good, flat
US 14	60% sepiolite – 40% boehmite	250	500 °C	good, flat
US 15	60% sepiolite – 40% boehmite	250	500 °C	good, flat
US 16	90% sepiolite – 10% boehmite	250	500 °C	cracks
US 17	90% sepiolite – 10% boehmite	250	500 °C	cracks

6.3.1 Results from Gas Permeation Experiments

The following gases underwent permeation tests at room temperature on the sepiolite membranes described above (except for US 16 and 17 that cracked and could not be tested): helium, nitrogen, carbon dioxide and methane. The membranes exhibited no selectivity for any of these gases.

These results showed that the attempts to create a tightly packed film of sepiolite (with or without boehmite as a binder) failed, and that the permeation took place through the space between fibers rather than through the microchannels along each fiber. An SEM picture of a pure sepiolite membrane calcined at 500 °C shows clearly its fibrous, paper-like structure (Figure 6.1), with no definite pore structure or pore size distribution.

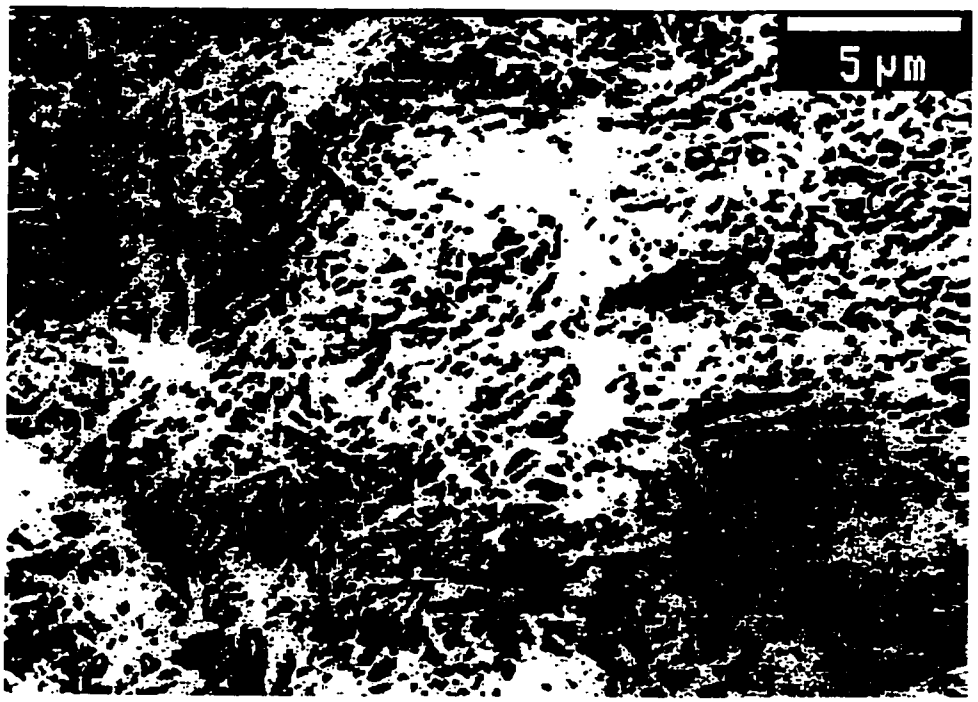

Figure 6.1. SEM Image of a 100% Sepiolite Membrane Calcined at 500 °C

By contrast, the same membrane (100% sepiolite) calcined at 765 °C shows a different picture, with the loose fibrous structure disappeared and replaced by a relatively uniform pore structure generated by a network of spheroidal particles sintered together (as seen in Figure 6.2).

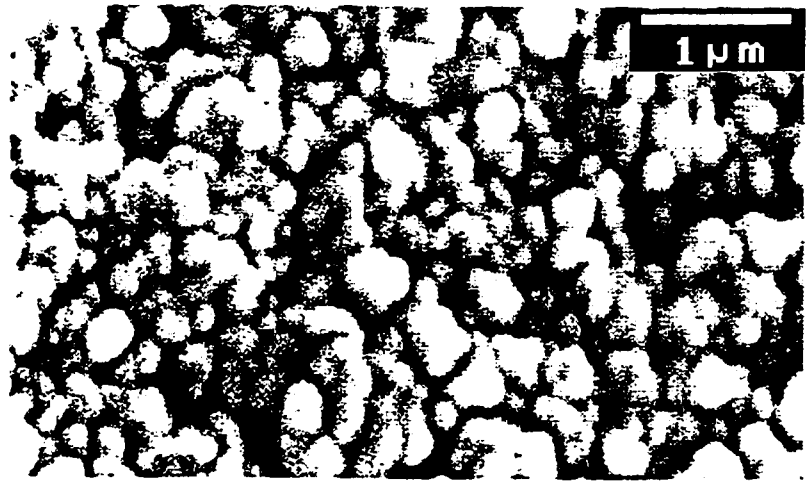

Figure 6.2. SEM Image of a 100% Sepiolite Membrane Calcined at 765 °C.

While the type of structure obtained was new and exciting, it was clear that this was not a gas separation membrane. This led to the decision to test this membrane in ultrafiltration experiments and perform a preliminary characterization and modeling. Ultrafiltration experiments were done as described in the section 5.5.1.2 and discussion follows.

6.3.2 Ultrafiltration Experiments with Sepiolite Membrane

Solutions of four narrowly dispersed molecular weights of poly (ethylene glycol) PEG and poly (ethylene oxide) PEO were prepared and used as feed solutions for ultrafiltration tests, as described in section 5.5.1.2.

The four molecular weights of solutes used were:

PEG M_w =35.000

PEO M_w =100,000

PEO M_w =200,000

PEO M_w =300,000

The Einstein-Stokes radii for PEG and PEO molecules of molecular weights specified above were calculated starting from the classic expression of the diffusivity of a molecule in a free solution, the Stokes-Einstein equation:

$$D = kT(6\pi\eta a)^{-1} \qquad 6.1$$

where: D is the diffusivity of the solute molecule (m^2/s)

η is the pure solvent viscosity (Pa s)

k is Boltzmann constant (J/K)

T is the absolute temperature (K)

a is the Einstein-Stokes radius of the solute molecule (m)

The diffusivities of PEG and PEO molecules in water could be found in the literature expressed empirically as functions of their intrinsic viscosity by the following equations (Hsieh et al., 1979):

$$D = 2.5\ kT\ \{10^{-6}\ \eta\ (M[\eta])^{1/3}\}^{-1} \qquad 6.2$$

where: D is the diffusivity of the solute molecule (m^2/s)

η is the pure solvent viscosity (Pa s)

k is Boltzmann constant (J/K)

T is the absolute temperature (K)

$[\eta]$ is the intrinsic viscosity of the solute in aqueous solution (m^3/kg)

M is the molecular weight of the solute (kg/kmol)

By combining the above two equations (Eq. 6.1 and Eq. 6.2), the following simplified relation could be obtained:

$$a = 2.122 \times 10^{-12}\ (M[\eta])^{1/3} \qquad 6.3$$

where: a is the Einstein-Stokes radius of the solute molecule (m)

M is its molecular weight (kg/kmol)

$[\eta]$ is the intrinsic viscosity of the solute (m^3/kg)

The intrinsic viscosity $[\eta]$of PEG could be calculated from the polymer's molecular weight M using the following empirical equation found in the literature (Meireles et al., 1995):

$$[\eta] = 4.9 \times 10^{-5} M^{0.672} \qquad 6.4$$

The intrinsic viscosity $[\eta]$of PEO could be calculated from the polymer's molecular weight M using the following empirical equation found in the literature (Nabi, 1968):

$$[\eta] = 1.192 \times 10^{-5} M^{0.76} \qquad 6.5$$

Intrinsic viscosities of PEG and PEO of various molecular weights calculated from the empirical equation shown above are in very good agreement with other experimental values found in the literature (Nabi, 1968; Hsieh et al., 1979; Meireles et al., 1995; Bessières et al., 1996; Singh et al., 1998)

By substituting the expression for intrinsic viscosity $[\eta]$ (Eq. 6.4 for PEG and Eq. 6.5 for PEO) in Eq. 6.3, the following final expressions of Einstein-Stokes radii of the solute molecules as functions of their molecular weight can be obtained:

For PEG:

$$a = 16.73 \times 10^{-12} M^{0.557} \qquad 6.6$$

for PEO:

$$a = 10.44 \times 10^{-12} M^{0.587} \qquad 6.7$$

The following table (Table 6.12) shows the calculated values of Einstein-Stokes radii for all solutes used.

Table 6.12. Calculated Values of Einstein-Stokes Radii for All Solutes Used

Solute	Stokes radius (nm)
PEG M_{w1} = 35,000	$a_1 = 5.7$
PEO M_{w2} =100,000	$a_2 = 9.0$
PEO M_{w3} =200,000	$a_3 = 13.5$
PEO M_{w4} =300,000	$a_4 = 17.1$

Concentration of the feed solutions was kept constant at 100 ppm for all permeation experiments.

6.3.3 Results

Separation was plotted versus solute molecular weight for all four testing pressures: 30 psig, 50 psig, 70 psig and 90 psig. These plots, also known as rejection curves, have the characteristic S-shape mentioned widely in the ultrafiltration literature. The graph for 50 psig transmembrane pressure is shown in Figure 6.3. Michaels (1980) was the first researcher that, based on the striking resemblance of these curves to the cumulative-particle-size-distribution curves for particulate solids, suggested a log-normal distribution function to correlate the separation with the Einstein-Stokes radius of the permeant's molecule. A log-normal distribution function was also used in modelling the present work and it was discussed in detail in Section 2.2.

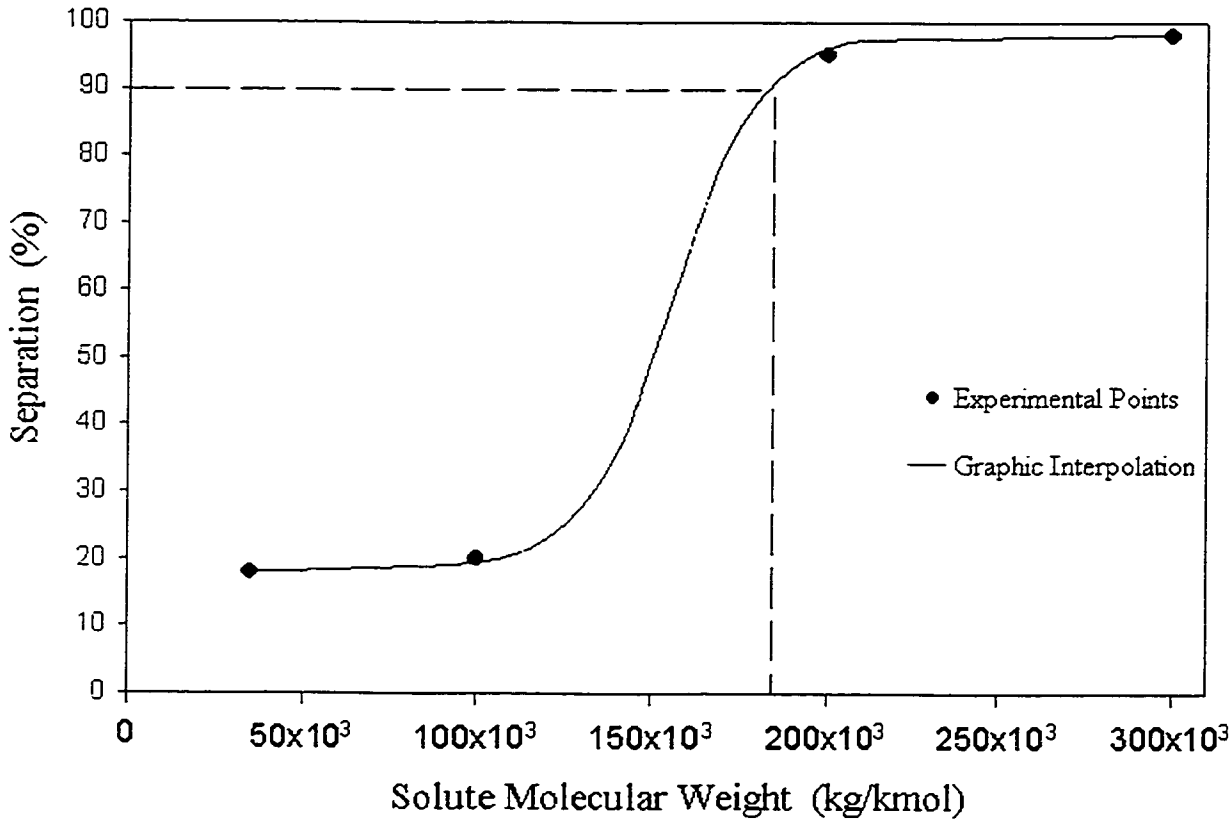

Figure 6.3. Separation versus Solute Molecular Weight for Sepiolite Membrane US 12. Experimental conditions: temperature: 22 °C, solute concentration in the feed: 100 ppm, transmembrane pressure: 50 psig.

From this plot the Molecular Weight Cut Off (MWCO) of the membrane was extrapolated. By definition, MWCO is the molecular weight of the solute that corresponds to a separation of 90%. As it can be seen from the plot, there is a sharp increase in the separation from a solute with M_w = 100,000 to a solute with M_w = 200,000. The MWCO extrapolated from the graph was 190,000 Daltons but, due to the inherent imprecision

associated with drawing a curve through just 4 points, it could be anywhere between 100,000 Daltons and 200,000 Daltons. This separation behaviour for the sepiolite membrane suggests a relatively narrow pore size distribution and a lack of defects and pinholes.

Solute separations were found to remain independent of the applied pressure, as seen in the graph shown in Figure 6.4:

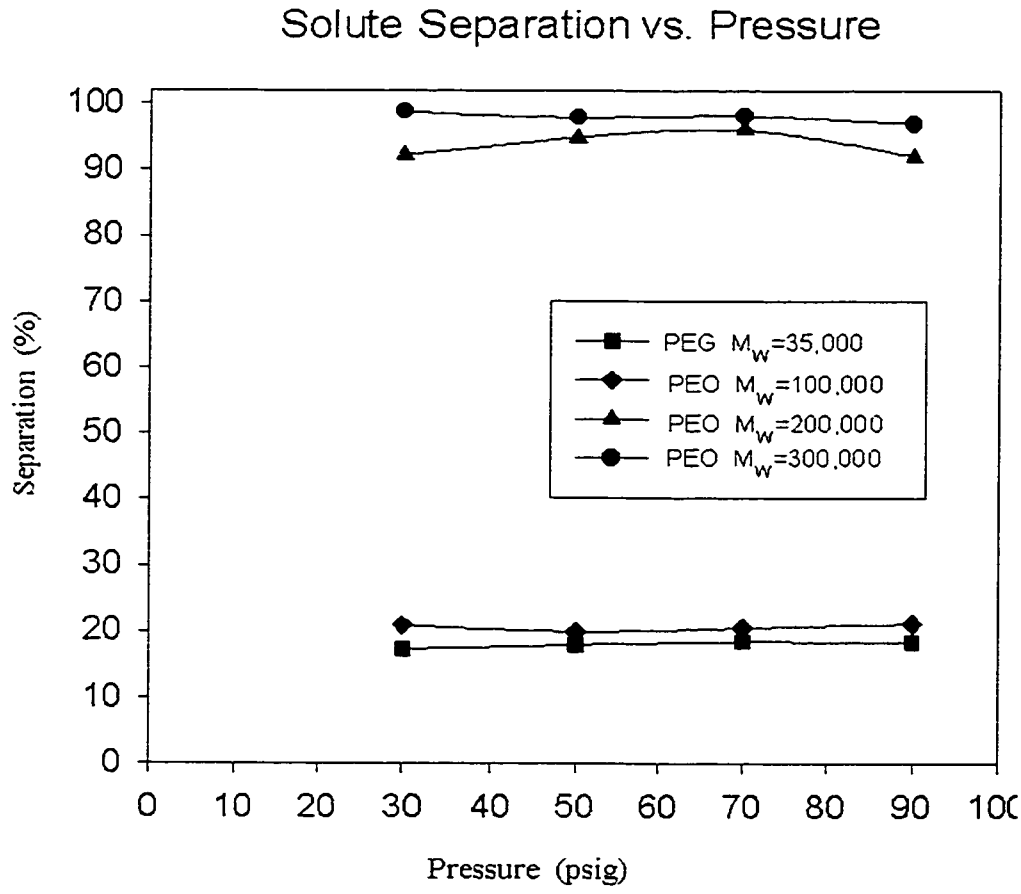

Figure 6.4. Solute Separation as a Function of Transmembrane Pressure for Sepiolite Membrane US 12. Experimental conditions: temperature: 22 °C, solute concentration in the feed: 100 ppm.

Permeate flux through membrane was found to increase linearly with the applied pressure; no flattening of the straight flux curves could be noticed, even at 90 psig transmembrane pressure, as it can be seen from Figure 6.5, which also includes pure water permeation flux:

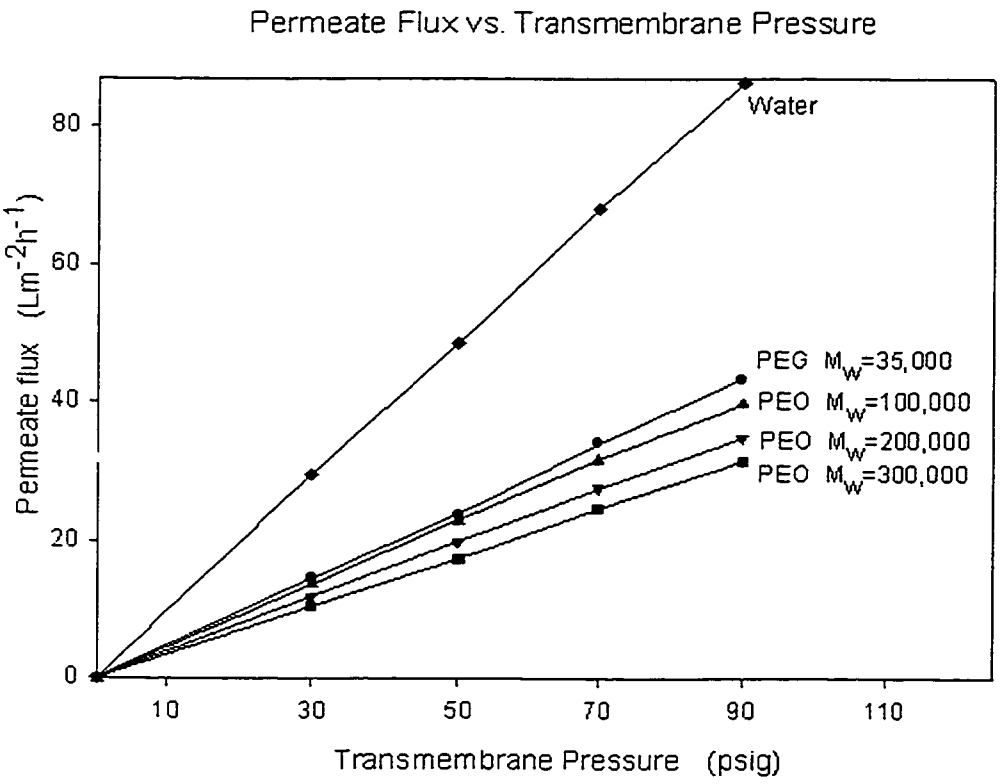

Figure 6.5. Permeate Flux versus Applied Pressure for Sepiolite Membrane US 12. Experimental conditions: temperature: 22 °C, solute concentration in the feed: 100 ppm (flux values corrected to 25 °C).

Permeate flux declined with an increase in the molecular weight of the solute, as seen in the graph shown in Figure 6.6, below:

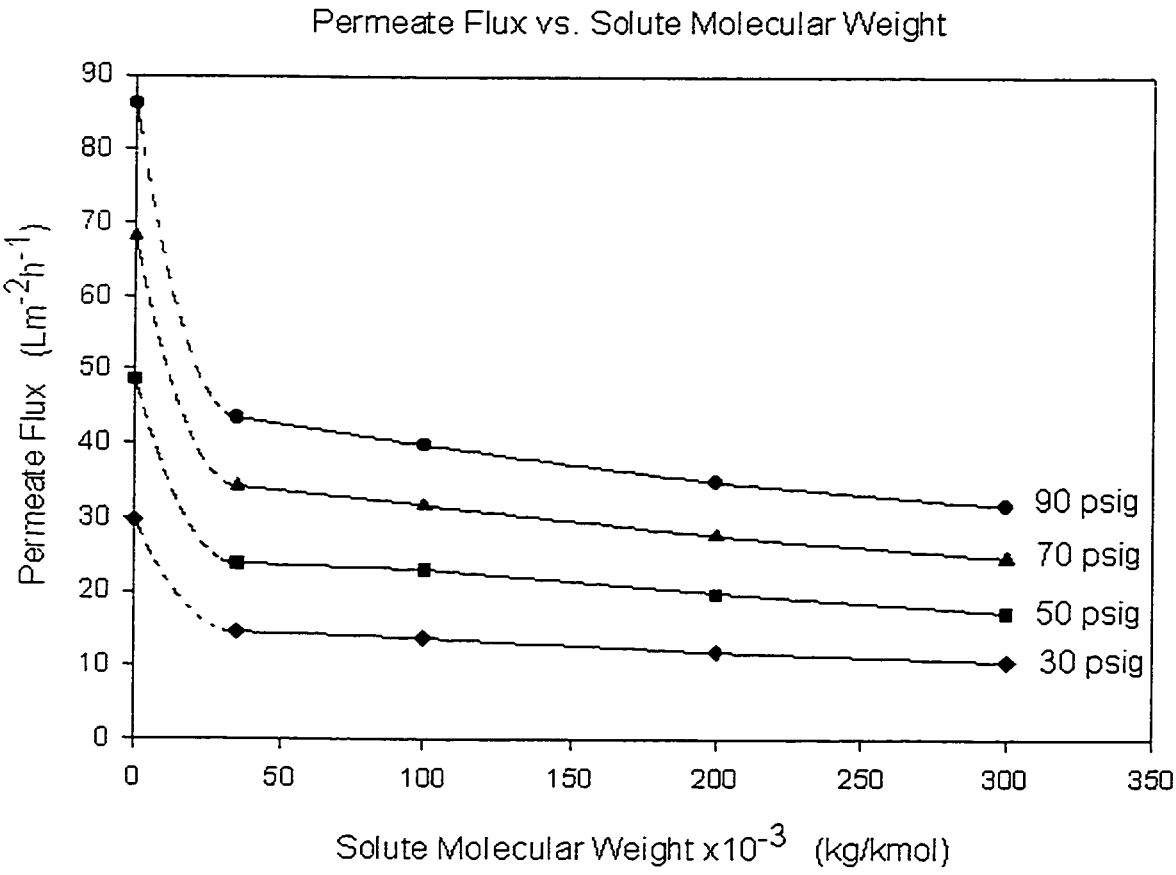

Figure 6.6. Permeate Flux versus Solute Molecular Weight for Sepiolite Membrane US 12. (flux values at molecular weight 0 kg/kmol represent pure water flux values and are included for reference only). Experimental conditions: temperature: 22 °C, solute concentration in the feed: 100 ppm (flux values corrected to 25 °C).

6.3.4 Discussion and Modelling

Four different solute molecule sizes were used for the experimental part *(n=4)*, therefore a set of eight equations with six unknowns is obtained from Eq. 2.10 and 2.13.

The known values in the equations above are the experimental and pre-set data shown in the next table (Table 6.13):

Table 6.13. Experimental and Measured Numeric Data Used as Inputs.

Solute molecular weight (kg/kmol)	Solute Stokes Radius a_i (nm)	Permeate Flux PR_i (l/m^2 h)	Flux ratio $\left(\frac{PR}{PWP}\right)_i$	Separation $(Sep)_i$
WATER		48.6		
PEG M_{w1} = 35,000	a_1 = 5.7	23.8	0.49	0.18
PEO M_{w2} =100,000	a_2= 9.0	23.0	0.47	0.20
PEO M_{w3} =200,000	a_3 = 13.5	19.8	0.41	0.95
PEO M_{w4} =300,000	a_4 = 17.1	17.3	0.36	0.98

Constant parameters:

Transmembrane pressure = 50 psig

Feed concentration = 100 ppm

Membrane area = 2.4 cm^2

Temperature = 295 K

For this set of eight equations with six unknowns, numerical solving and regression analysis was performed using an algorithm available as an IMSL (International Mathematics Subroutine Library).

The results are shown below:

$\bar{r}$ = 9.34 nm

σ = 1.374

r_1 = 11.5 nm

r_2 = 12.7 nm

r_3 = 16.9 nm

r_4 = 18.2 nm

Correlation coefficient was found to be $\rho^2 = 0.84$.

The following four graphs (Figure 6.7 through 6.10) show the membrane pore size distribution according to this model and the blocked pores distribution (grey area) for each solute.

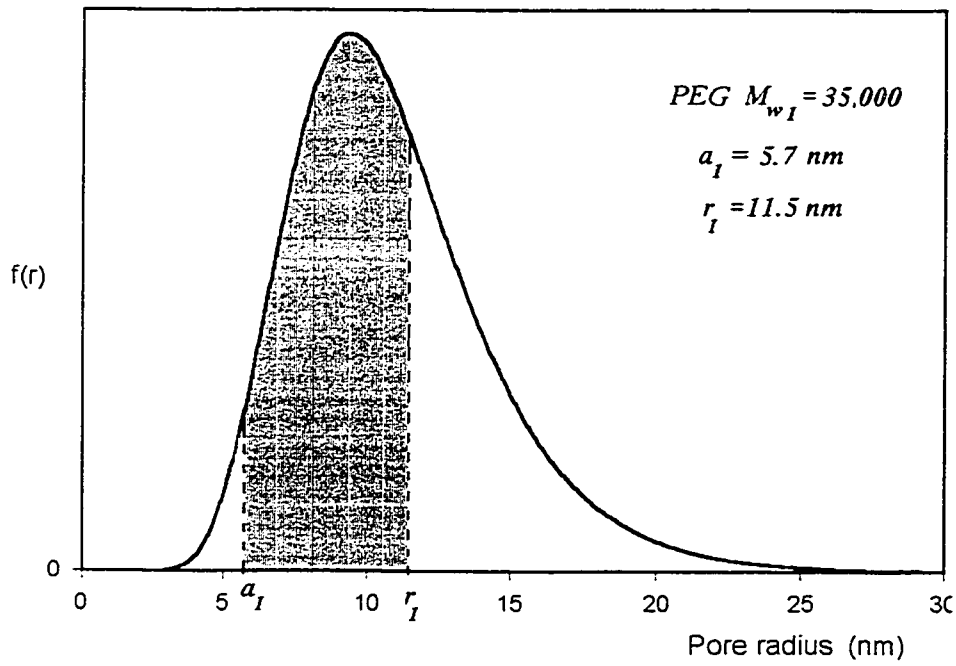

Figure 6.7. Membrane Pore Size Distribution and Blocked Pores in the Case of PEG (M_w=35.000) as Transported Solute.

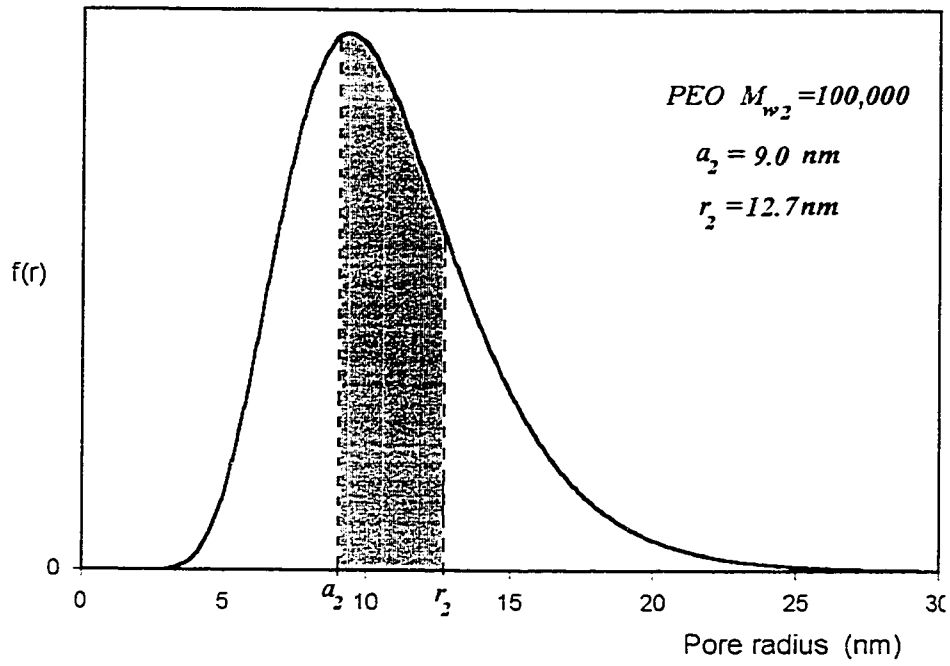

Figure 6.8. Membrane Pore Size Distribution and Blocked Pores in the Case of PEO (M_w=100.000) as Transported Solute.

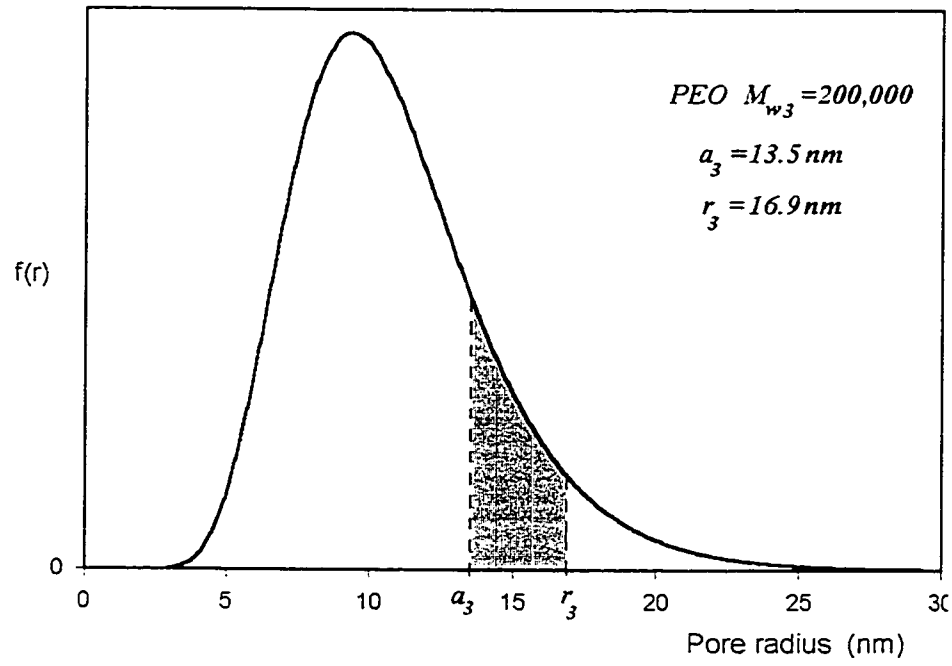

Figure 6.9. Membrane Pore Size Distribution and Blocked Pores in the Case of PEO (M_w=200,000) as Transported Solute.

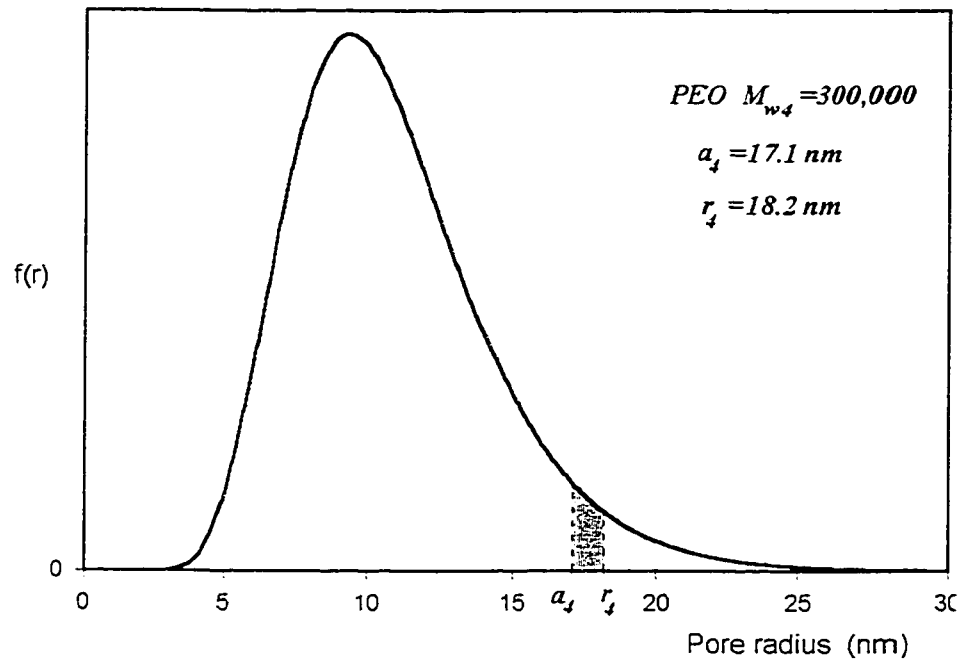

Figure 6.10. Membrane Pore Size Distribution and Blocked Pores in the Case of PEO (M_w=300,000) as Transported Solute.

The values of separation and flux ratio calculated according to the model are shown in the Table 6.14. It can be noticed that the model underestimates slightly the flux ratios for the two highest molecular weight solutes and overestimates them for the two lowest molecular weight solutes. Separation values predicted by the model are slightly below the experimental values for all solutes except the PEO with M_w of 100,000 kg/kmol, for which the model predicts a higher value.

Table 6.14. Values of Separation and Flux Ratios Calculated According to the Model.

Solute	Flux Ratio Predicted by the Model	Separation Predicted by the Model
PEG M_{w1} = 35,000	0.58	0.14
PEO M_{w2} =100,000	0.54	0.23
PEO M_{w3} =200,000	0.38	0.89
PEO M_{w4} =300,000	0.31	0.94

The sharp molecular weight cut off exhibited by these membranes can be explained by the value of $\bar{r}$ and σ, the average pore size and the standard deviation of the pore size distribution, as calculated. Since, according to the model used, most of the pore sizes are quite narrowly spaced in the range of 9 to 10 nm, it seems logical that solute molecules of 13.5 nm radius (as those of PEO with a M_w = 200,000 kg/kmol) find passage through pores

much more difficult compared to smaller solute molecules (e.g. PEO with a M_w = 100,000 kg/kmol, which measure 9.0 nm in radius).

As for the pore blocking situation, one trend that can be noticed from the four graphs shown above is that a marked shift (from small to large)in the blocked pore size takes place as the solute size increases. For the case of PEG (M_w = 35,000), the maximum size of the blocked pores is 11.5 nm, which is roughly twice the size of solute molecule size (5.7 nm); a monomolecular adsorption layer on the pore walls could be the explanation. For all other three solutes, the ratio of the maximum blocked pore size to solute molecule size is smaller than 2.0 and is decreasing as the solute size increases. No obvious explanation for this trend could be found; among the possible causes: deviations from monodispersity in the polymers used as solutes, strong hydrogen bond interactions between the oxygen atoms from the polymer and the hydroxyl groups present on the clay surface, membrane imperfections (microcracks, pinholes, uneven thickness) and, of course, the simplifying assumptions made in the model chosen.

Chapter 7. CONCLUSIONS AND RECOMMENDATIONS

As mentioned in the introduction, the main goal of this project was of an exploratory nature and, as such, its achievements were not necessarily the ones carefully planned ahead. The unsupported pillared montmorillonite/boehmite membranes proved to have good gas separation properties but a frail and cumbersome physical structure, which constituted its major drawback. All efforts towards finding a suitable support for this material did not succeed. If future work is carried out into finding a good support for a thin, air-tight layer of this material, it could become a serious candidate for a satisfactory high temperature membrane module. Also, more work would be needed with regards to its stability at higher temperatures, stability under steam conditions, the possibility of imparting catalytic properties to the membrane material (without affecting its separation performance) and the possibility of fine-tuning its pore size (e.g. by using different pillaring agents).

The sepiolite membrane was also, unexpectedly, a good ultrafiltration membrane and not a gas separation membrane as initially envisioned. Since the preliminary testing showed good separation properties, it is recommended that further work be carried on in this direction. An area of interest could be the preparation of supported membranes of this type. Also shapes other than flat sheets could be attempted.

BIBLIOGRAPHY

1. Ahlrichs, J.L., Serna, C., Serratosa, J.M., Clays and Clay Min., **23**, 119 (1975)

2. Bai, C., Jia, M.D., Falconer, J.L., Noble, R.D., Preparation and separation properties of silicalite composite membranes, J. Membrane Sci., **105**, 79 (1995)

3. Baykara, T., Gunay, E., Kara, M., Tarar, S.S., Microstructural development during the sintering of sepiolite, Key Eng. Mater., **132-136**, 872-75 (1997)

4. Bjorkert, U.S., Holland, D., Lewis, M.H., Phase development in sol derived microporous membranes for gas permselectivity, J. Sol-Gel Sci. Technol., **13**, 799-803 (1998)

5. Bjorkert, U.S., Mayappan, R., Holland, D., Lewis, M.H., Phase development in La_2O_3 doped Al_2O_3/TiO_2 ceramic membranes, J. Euro. Ceramic Soc., **19**, 1847-1857 (1999)

6. Caillere, S., Henin, S., in Brown, G. (Ed.), The X-ray Identification and Crystal Structures of Clay Minerals, Mineralogical Society, London, (1961)

7. Cheong, H.C., Ha, J.-S., Kim, C.-S., Choi, D.-K., Cheong, D.-S., Structural evolution of alumina membrane prepared on an alumina support using a sol-gel method, Journal of Alloys & Compounds, **290**, 304-309 (1999)

8. Chau, J.L.H., Tellez, C., Yeung, K.L., Ho, K.C., The role of surface chemistry in zeolite membrane formation, J. Membrane Sci., **164**, 257-275 (2000)

9. Cho, Y-K., Han, K., Lee, K-H., J. Membrane Sci., **104**, 219-230 (1995)

10. Corma, A., Perez-Parien, J., Forna, V., Mifsud, A., Clay Miner., **19**, 673 (1984)

11. De Lange, R.S.A., Hekkink, J.H.A., Keizer, K., Burggraaf, A.J., Formation and characterization of supported microporous ceramic membranes prepared by sol-gel modification techniques, J. Membrane Sci., **99**, 57 (1995)

12. De Lange, R.S.A., Keizer, K., Burggraaf, A.J., Analysis, and theory of gas transport in microporous sol-gel derived ceramic membranes, J. Membrane Sci., **104**, 81 (1995)

13. Fernandes Alvares, T., Clay Miner., **13**, 375 (1978)

14. Fernandes Hernandes, M.N., Ruiz-Hitzky, E., Clay Miner., **14**, 295 (1979)

15. Fu, G., Nazar, L.F., Bain, A.D., Chem. Mater., **3**, 602-610, (1991)

16. Fukushima, Y., Meng, X., Yanagisawa, K., Yamasaki, N., J. Jap. Soc. Powder & Powder Metallurgy, **40**, 355 (1993)

17. Goktas, A.A., Misirli, Z., Baykara, T., Ceramics Int., **23**, 305 (1997)

18. Grillet, Y., Cases, J.M., Francois, M., Rouquerol, J., Poirier, J.E., Clays and Clay Min., **36**, 233 (1988)

19. Hassan, M.H., Way, J.D., Thoen, P.M., Dillon, A.C., Single component and mixed gas transport in a silica hollow fibre membrane, J. Membrane Sci., **104**, 27 (1995)

20. Honma, I., Takeda, Y., Bae, J.M., Protonic conducting properties of sol-gel derived organic/inorganic nanocomposite membranes doped with acidic functional molecules, Solid State Ionics, **120**, 255-264 (1999)

21. Hsieh, F.-U., Matsuura, T., Sourirajan, S., Reverse osmosis separations of polyethylene glycols in dilute aqueous solutions using porous cellulose acetate membranes, J. Appl. Polym. Sci., **23**, 561-573 (1979)

22. Hu, Z-H., Zhu, H-Y., Vansant, E.F., Separation of nitrogen and organic vapors by pillared clay-carbon composite membrane; Proc. Technol., Proc., (Separation Technology), **11**, 567-571 (1994)

23. Jarayaman, V., Lin, Y.S., Synthesis and hydrogen permeation properties of ultra thin palladium-silver alloy membranes. J. Membrane Sci., **104**, 251 (1995)

24. Jiang, S., Yan, Y., Gavalas, G.R., Temporary carbon barriers in the preparation of H_2-permselective silica membranes, J. Membrane Sci., **103**, 211 (1995)

25. Kusakabe, K., Sakamoto, S., Saie, T., Morooka, S., Pore structure of silica membranes formed by a sol-gel technique using tetraethoxysilane and alkyltriethoxysilanes, Sep. Purif. Technol., **16**, 139-146 (1999)

26. Lao, H., Detellier, C., Matsuura, T., Tremblay, A.Y., Microporous inorganic membranes - preparation by the sol- gel process and characterization of unsupported composite membranes of alumina and polyoxoaluminium pillared montmorillonite; J. Mater. Sci. Lett., **13**, 895-897, (1994)

27. Lao, H., Development of Pillared Clay Membranes for the Separation of Hexanes and Its Isomers (Final Report – Contract No. 23440-2-9198/01-SQ)

28. Lee, J.-H., Choi, S.-C., Bae, D.-S., Han, K.-S., Synthesis and microstructure of silica-doped alumina composite membrane by sol-gel process, J. Mater. Sci. Lett., **18**, 1367-1369 (1999)

29. Meireles, M., Bessieres, A., Rogissart, I., Aimar, P., Sanchez, V., An appropriate molecular size parameter for porous membranes calibration, J. Membr. Sci., **103**, 105-115 (1995)

30. Michaels, A.S., Analysis and prediction of sieving curves for ultrafiltration membranes: A universal correlation?, Sep. Sci. Techol., **15**, 1305-1322 (1980)

31. Morooka, S., Yan, S., Kusakabe, K., Akiyama, Y., Formation of hydrogen permselective SiO_2 membrane in macropores of alpha alumina support tube by thermal decomposition of tetraethylorthosilicate, J. Membrane Sci., **101**, 89 (1995)

32. Nagata, H., Shimoda, S., Sudo, T., Clays and Clay Min., **22**, 285 (1974)

33. Pan, M., Cooper, C., Lin, Y.S., Meng, G.Y., CVD modification and vapor/gas separation properties of nanoporous alumina membranes, J. Membrane Sci., **158**, 235-241 (1999)

34. Raman, N. K., Brinker, C.J., Organic template approach to molecular sieving silica membranes, J. Membrane Sci., **105**, 273 (1995)

35. Rautureau, M., Tchoubar, C., Clays and Clay Min., **24**, 285 (1976)

36. Reed, J.S., Introduction to the Principles of Ceramic Processing, Wiley, New York, 1989

37. Rezgui, S., Gates, B.C., Burkett, S.L., Davis, M.E., Chem. Mater., **6**, 2390-2397 (1994)

38. Rubica, E.H., Clay Miner., **20**, 525 (1985)

39. Santaren, J., Modern Paint and Coatings, 68 (1993)

40. Schaep, J., Vandecasteele, C., Peeters, B., Luyten, J., Dotremont, C., Roels, D., Characteristics and retention properties of a mesoporous gamma -Al_2O_3 membrane for nanofiltration, J. Membrane Sci., **163**, 229-237 (1999)

41. Schiza, M.V., Nivens, D.A., Milanovich, F.P., Angel, S.M., Characterization of mixed TiO_2 and SiO_2 sol-gel membranes for volatile organochloride sensing, Proc. Spie - Int. Soc. Optic. Eng., **3540**, 164-174 (1999)

42. Schlottig, F., Textor, M., Georgi, U., Roewer, G., Template synthesis of SiO_2 nanostructures, J. Mater. Sci. Lett., **18**, 599-601 (1999)

43. Seshadri, K S., Ahmed, J., Kesavamoorthy, R., Varatharajan, K., Srinivasan, M.P., Krishnasamy, V., Estimation of pore charge on zirconia membrane prepared by sol-gel route using zeta potential measurement, J. Mater. Sci. Technol., **14**, 425-428 (1998)

44. Shi, L., Wong, N.-B., Tin, K.-C., Chung, C.-Y., Thermal stability of TiY membrane, J. Mater. Sci., **34**, 2789-2792 (1999)

45. Shusen, W., Meiyun, Z., Zhizhong, W., Asymmetric molecular sieve carbon membranes, J. Membrane Sci., **109**, 267 (1995)

46. Simonton, T.C., Komarneni, S., Roy, R., Appl. Clay Sci., **3**, 165 (1998)

47. Tsapatis, M., Gavalas, G., Structure and aging characteristics of H_2-permselectve SiO_2 – Vycor membranes, J. Membrane Sci., **87**, 281 (1994)

48. Uhlhorn, R. J. R., Huis In't Veld, M.H.B.J., Keizer, K., J. Mater. Sci., **27**, 527-537 (1992)

49. Vacassy, R., Guizard, C., Palmeri, J., Cot, L., Influence of the interface on the filtration performance of nanostructured zirconia ceramic, Nanostructured Materials, **10**, 77-88 (1998)

50. Vercauteren, S., Keizer, K., Vansant, E.F., Luyten, J., Leysen, R., Porous ceramic membranes: Preparation, transport properties and applications, J. Porous Mater., **5**, 241-258 (1998)

51. Vercauteren, S., Vayer, M., Van Damme, H., Luyten, J., Leysen, R., Vansant, E.F., Preparation and characterization of ceramic membranes with a pillared clay top layer, Colloids & Surfaces A-Physicochemical & Engineering Aspects, **138**, 367-376 (1998)

52. Vercauteren, S., Luyten, J., Leysen, R., Vansant, E.F., Synthesis and characterization of a pillared clay membrane, J. Membrane Sci., **119**, 161-168 (1996)

53. Wu, J.K.S., Sabol, H., Smith, G.W., Flowers, D.L., Liu, P.K.T., Characterization of hydrogen-permselective microporous ceramic membranes, J. Membrane Sci., **96**, 275 (1994)

54. Xia, C., Cao, H., Wang, H., Yang, P., Meng, G., Peng, D., Sol-gel synthesis of yttria stabilized zirconia membranes through controlled hydrolysis of zirconium alkoxide, J. Membrane Sci., **162**, 181-188 (1999)

55. Yang, W.P., Shyu, S.S., Lee, E.-S., Chao, A.-C., Effects of PVA content and calcination temperature on the properties of PVA/boehmite composite film, Mater. Chem. Phys., **45**, 108-113 (1996)

56. Zhua, B., Fast ionic conducting film ceramic membranes with advanced applications, Solid State Ionics, **119**, 305-310 (1999)